



Deposited via The University of Sheffield.

White Rose Research Online URL for this paper:

<https://eprints.whiterose.ac.uk/id/eprint/169950/>

Version: Accepted Version

Article:

Hepworth, C., Wood, W.H.J., Emrich-Mills, T.Z. et al. (2021) Dynamic thylakoid stacking and state transitions work synergistically to avoid acceptor-side limitation of photosystem I. *Nature Plants*, 7 (1). pp. 87-98. ISSN: 2055-026X

<https://doi.org/10.1038/s41477-020-00828-3>

This is a post-peer-review, pre-copyedit version of an article published in *Nature Plants*. The final authenticated version is available online at: <https://doi.org/10.1038/s41477-020-00828-3>.

Reuse

Items deposited in White Rose Research Online are protected by copyright, with all rights reserved unless indicated otherwise. They may be downloaded and/or printed for private study, or other acts as permitted by national copyright laws. The publisher or other rights holders may allow further reproduction and re-use of the full text version. This is indicated by the licence information on the White Rose Research Online record for the item.

Takedown

If you consider content in White Rose Research Online to be in breach of UK law, please notify us by emailing eprints@whiterose.ac.uk including the URL of the record and the reason for the withdrawal request.

Dynamic thylakoid stacking and state transitions work synergistically to avoid acceptor-side limitation of photosystem I

Christopher Hepworth¹, William H.J. Wood¹, Tom Z. Emrich-Mills¹, Matthew S. Proctor¹, Stuart Casson¹ and Matthew P. Johnson¹

¹Department of Molecular Biology and Biotechnology, University of Sheffield, Firth Court, Western Bank, Sheffield, S10 2TN, United Kingdom.

*=Corresponding author matt.johnson@sheffield.ac.uk

Abstract

TAP38/STN7-dependent (de)phosphorylation of light harvesting complex II (LHCII) regulates the relative excitation rates of photosystems I and II (PSI, PSII) (state transitions) and the size of the thylakoid grana stacks (dynamic thylakoid stacking). Yet, it remains unclear how changing grana size benefits photosynthesis and whether these two regulatory mechanisms function independently. Here by comparing *Arabidopsis* wild-type, *stn7* and *tap38* plants with the *psal* mutant, which undergoes dynamic thylakoid stacking but lacks state transitions, we elucidate their distinct roles. Under low light, smaller grana increase the rate of PSI reduction and photosynthesis by reducing the diffusion distance for plastoquinol, however this beneficial effect is only apparent when PSI/PSII excitation balance is maintained by state transitions or far-red light. Under high light, the larger grana slow plastoquinol diffusion and lower the equilibrium constant between plastocyanin and PSI, maximising photosynthesis by avoiding PSI photoinhibition. Loss of state transitions in low light or maintenance of smaller grana in high light also both bring about a decrease in cyclic electron transfer and over-reduction of the PSI acceptor-side. These results demonstrate that state transitions and dynamic thylakoid stacking work synergistically to regulate photosynthesis in variable light.

35

36 **Introduction**

37 Natural environments expose plants to large and rapid variations in light intensity¹. These can
38 cause mismatches between the rate of photosynthetic electron transfer and the capacity of
39 downstream electron sinks, such as the CO₂-fixing Calvin-Benson-Bassham (CBB) cycle².
40 The build-up of electrons on the acceptor-sides of photosystems I and II (PSI and PSII) can
41 damage the delicate reaction centres by promoting formation of reactive oxygen species
42 (ROS)³. Fortunately, plants possess an extensive armoury of regulatory mechanisms,
43 allowing them to cope with fluctuations in light intensity and avoid, or minimise, photo-
44 oxidative stress. PSII is protected by non-photochemical quenching (NPQ), wherein excess
45 absorbed solar energy in the light harvesting antenna complexes (LHCII) is safely dissipated
46 as heat⁴. PSI is protected primarily by photosynthetic control, which avoids over-reduction of
47 the acceptor-side by regulating the rate of electron donation from the cytochrome *b₆f* (*cytb₆f*)
48 complex via plastocyanin (Pc)⁵. NPQ and photosynthetic control are induced in high light by
49 the build-up of the transmembrane Δ pH that results from coupled linear and cyclic electron
50 transfer (LET and CET)⁴⁻⁶. While LET involves transfer of electrons from water to NADP⁺
51 via PSII, plastoquinone (PQ), *cytb₆f*, Pc, PSI, ferredoxin (Fd) and ferredoxin-NADP⁺
52 reductase (FNR), CET recycles electrons from Fd back to the PQ pool, contributing to Δ pH
53 and ATP synthesis without net NADP⁺ reduction. In *Arabidopsis* Fd-PQ reductase (FQR)
54 activity is associated with two separate pathways, the first involves photosynthetic complex I
55 (NDH) and the second involves the PGR5 and PGRL1 proteins and is sensitive to the
56 inhibitor antimycin-A (AA)^{6,7}. PGR5 and PGRL1 have been suggested to function directly as
57 the AA-sensitive FQR⁸ or act as regulators of FQR activity by an FNR-*cytb₆f* complex^{9,10}.
58 Since Δ pH forms and relaxes on a timescale of seconds, NPQ and photosynthetic control are
59 able to rapidly track light intensity^{2,4,5}. In addition, plants can regulate photosynthesis by

60 modulating the redox state of the photosynthetic electron transfer chain via the reversible
61 phosphorylation of LHCII^{11,12}. In contrast to photosynthetic control and NPQ, this
62 mechanism occurs on timescales of minutes to tens of minutes, so is likely to integrate
63 changes in light intensity and spectral quality over a longer period. The stromal-facing N-
64 termini of the LHCb1 and LHCb2 subunits of LHCII are phosphorylated by the serine-
65 threonine kinase STN7 and dephosphorylated by the phosphatase TAP38 (PPH1)¹³⁻¹⁵. In low
66 light STN7 is activated by the binding of plastoquinol (PQH₂) to the oxidising site of the
67 *cytb_f* complex¹⁶. In high light, STN7 is inactivated by the build-up of reduced thioredoxin in
68 the stroma and/or the ΔpH ^{17,18}. Since TAP38 is believed to be constitutively active, the
69 activity of STN7 thereby determines the steady state phosphorylation level of LHCII^{14,15}.
70 Loss of LHCII phosphorylation, NPQ or photosynthetic control is associated with reduced
71 plant growth and yield in fluctuating light, characteristic of natural environments¹⁹⁻²².

72 When LHCII is dephosphorylated the majority is energetically coupled to PSII (State
73 I). Phosphorylation results in an increased proportion of LHCII becoming energetically
74 coupled to PSI via its PSAL/H/O subunits (State II)²³. In this way phosphorylation regulates
75 the relative excitation rates of PSI and PSII to ensure efficient operation of the LET chain, a
76 mechanism known as the state transition^{11,12}. Since State II increases PSI/ PSII excitation
77 ratio it was also suggested as a mechanism to increase the CET to LET ratio and therefore the
78 supply of ATP relative to NADPH²⁴⁻²⁷. It is clear however that CET does not obligatorily
79 depend on state transitions in either *Arabidopsis* or *Chlamydomonas*^{28,29}. LHCII
80 phosphorylation also affects the organization of the thylakoid membrane by controlling the
81 interactions between the stromal faces of LHCII complexes that sustain grana stacking³⁰.
82 Phosphorylation in low light promotes a reduction in the number of membrane layers and
83 diameter of the grana stacks, while increasing the number of grana per chloroplast;
84 dephosphorylation in high light provokes the opposite response³¹⁻³⁴. Unlike state transitions,

85 the function of dynamic thylakoid stacking is not well established. Smaller grana were
86 suggested to facilitate the exchange of phosphorylated LHCII between grana and stromal
87 lamellae³⁰. Recent theoretical work showed that larger grana increase light scattering relative
88 to absorption, thus potentially acting as a photoprotective mechanism in high light³⁵. Using
89 absorption flash spectroscopy, we recently demonstrated that reducing grana size increased
90 the rate of PSI reduction in spinach, and suggested this could increase LET efficiency³³. In
91 contrast, we found that PSI reduction following far-red illumination was enhanced in larger
92 grana, consistent with an increased capacity for CET^{10,33}. We therefore hypothesised that
93 dynamic thylakoid stacking could act as mechanism to control the CET to LET ratio, though
94 in this case the dephosphorylated state would favour CET³³.

95 The absence of LHCII phosphorylation in the *stn7* mutant under low light conditions
96 leads to an over-reduction of the PQ pool and acceptor-side limitation of PSII, reducing LET
97 ³⁶⁻³⁸. However, to date no obvious penalty has been demonstrated for the maintenance of
98 LHCII phosphorylation in high light in the *tap38* mutant. Moreover, it remains unclear
99 whether dynamic thylakoid stacking affects photosynthetic efficiency in the steady state and
100 whether it can act independently of state transitions. In this study we compared the behaviour
101 of wild-type (WT), *stn7* and *tap38 Arabidopsis* plants with the *psal* mutant, which lacks state
102 transitions but retains dynamic thylakoid stacking, to better understand how LHCII
103 phosphorylation regulates photosynthesis in low and high light.

104

105 **Grana size and state transitions in WT, *psal*, *stn7* and *tap38***

106 Previously dynamic thylakoid stacking has been studied under broadband white light ³¹⁻³³;
107 hence we first sought to establish if this phenomenon was also observable under the 635 / 460
108 nm light combination employed by the infra-red gas exchange, absorption spectroscopy and
109 chlorophyll fluorescence instruments used in the following experiments. Using structured

110 illumination microscopy (SIM) we assessed grana size in low light (LL, 125 $\mu\text{mol photons m}^{-2}$
111 s^{-1}) and high light (HL, 1150 $\mu\text{mol photons m}^{-2} \text{s}^{-1}$) (Fig 1A). The mean grana diameter, as
112 measured by the full width half maximum (FWHM) of the fluorescence signal of each
113 granum, was significantly smaller in WT, *psal* and *tap38* in LL compared to *stn7*, while in
114 HL the *psal*, WT and *stn7* were larger than *tap38* (Fig 1B). Using 77K fluorescence emission
115 spectroscopy we compared the relative antenna size change of PSI between LL and HL in
116 WT and the mutants (Fig 1C). In the WT there is a decrease in the F735 (PSI)/F685 (PSII)
117 fluorescence ratio between LL and HL conditions consistent with a State II to I transition as
118 STN7 is inactivated in HL (Fig. 1C). However, no difference is seen in either *stn7* or *psal*,
119 which remained locked in State I in both LL and HL with a low F735/F685 ratio and *tap38*
120 that remained locked in State II (Fig. 1C)^{13,14,23,39}. These differences in the relative PSI/PSII
121 antenna size were confirmed using absorption and fluorescence spectroscopy (Extended Data
122 Fig. 1).

123

124 **Effect of grana size and state transitions on photosynthesis**

125 We next used infra-red gas exchange and chlorophyll fluorescence imaging to assess the
126 photosynthetic properties of the mutants in low light (LL, 125 $\mu\text{mol photons m}^{-2} \text{s}^{-1}$) and high
127 light (1150 $\mu\text{mol photons m}^{-2} \text{s}^{-1}$). After 10 minutes of LL illumination, CO_2 assimilation
128 (A^{14}CO_2) was higher in WT and *tap38* compared to *stn7* and *psal* (Fig. 2A). On the other hand,
129 in HL *tap38* showed significantly lower A^{14}CO_2 than *stn7*, WT and *psal* (Fig. 2A). These
130 effects were not due to differences in stomatal density or conductance, which were similar
131 among the mutants and WT (Extended Data Fig. 2). Chlorophyll fluorescence imaging
132 showed that the PSII quantum yield (ΦPSII) was lowest in *psal* and *stn7* in LL, while in HL
133 it was lowest in *tap38* (Fig. 2B). While the inferior A^{14}CO_2 and ΦPSII of *stn7* and *psal* in LL is
134 expected^{13,36,37}, the inferior performance of *tap38* in HL has not, to our knowledge, been

135 previously reported. Using chlorophyll fluorescence and P700 absorption spectroscopy we
136 next subjected plants to 10 minutes of LL illumination, briefly augmented for 30 seconds
137 with far-red (FR) light (740 nm, 255 $\mu\text{mol photons m}^{-2} \text{ s}^{-1}$) between the 400-430 second time
138 points, followed by 10 minutes of HL, and finally 4 minutes of dark relaxation (Fig. 2C-H).
139 The 30 seconds of FR is sufficient to reach a steady state level of P700 oxidation⁴⁰, but
140 insufficient to reverse LHCII phosphorylation and cause reversion to State I, a process which
141 takes ~15-30 minutes^{11,12}. Under LL illumination the ΦPSII initially decreased in all plants,
142 but then rose in the subsequent minutes as the CBB cycle and downstream electron sinks
143 were activated and the transient NPQ relaxed (Fig. 2C and E). The NPQ transient was largest
144 in *stn7* and smallest in *tap38* (Fig. 2E). ΦPSII was highest in *tap38* after ~100 seconds, while
145 in subsequent 100-200 seconds the WT rose to the same level, consistent with the transition
146 to State II. *Psal* and *stn7*, which are locked in State I, showed a ~20% lower ΦPSII , which
147 did not increase further (Fig. 2C). Augmentation of LL with FR for 30 seconds transiently
148 increased ΦPSII in *psal* to WT/*tap38* levels but had a significantly diminished restorative
149 effect in *stn7* (Fig. 2C). The lower ΦPSII under LL in *stn7* and *psal* was accompanied by an
150 increased reduction of the PSII acceptor Q_A (measured as 1-qL) compared to *tap38* and WT.
151 This effect is likely caused by inefficient oxidation of the PQ pool by PSI (via *cytb₆f*) due to
152 its under-excitation relative to PSII in the *stn7* and *psal* plants (Fig. 2D). Consistent with this
153 idea augmentation of LL with FR lowered 1-qL in *psal* and *stn7*, however the effect was
154 smaller in the latter (Fig. 2D). Since the level of PSI and Pc:PSI ratios are similar in *psal* and
155 *stn7* (Extended Data Fig. 3) their differential performance in LL + FR indicates that the latter
156 has some additional disadvantage that cannot be corrected by boosting PSI excitation. As in
157 PSII, the PSI quantum yield (ΦPSI) transiently decreased when LL illumination commenced,
158 and this was coincident with a transient rise in the PSI donor side limitation ($Y(\text{ND})$) (Fig. 2F
159 and G). ΦPSI rose as the CBB cycle was activated and was highest in *tap38*; by 250 seconds

160 the WT rose to a level not significantly different (Fig. 2F). Rising Φ PSI in all plants was
161 mirrored by a decrease in the PSI acceptor side limitation (Y(NA)) (Fig. 2H). The Φ PSI and a
162 Y(NA) values in the *stn7* and *psal* mutants began to diverge gradually from the wild-type
163 from 250 s onwards during the LL period and after ~400 s they were significantly different
164 (Fig. 2F and H). Increased Y(NA) in *stn7* relative to WT agrees with previous observations
165 made in low and fluctuating light³⁶. FR decreased the Φ PSI in all plants but simultaneously
166 decreased Y(NA), while Y(ND) increased (Fig. 2F, G and H). This effect is in line with the
167 preferential excitation of PSI with FR, which oxidises the inter-system electron transfer chain
168 inducing a donor-side limitation. While Φ PSI falls under FR, the additional excitation will
169 nonetheless stimulate the rate of PSI electron transfer⁴¹. Notably, in *stn7* the Y(ND) is higher
170 under LL + FR than in *psal* (Fig. 2G). Therefore, only when the limitation of PSI oxidation
171 rate in LL is lifted by state transitions or FR augmentation can a beneficial effect of smaller
172 grana be observed.

173 The lower $^A\text{CO}_2$ and Φ PSII in *tap38* under HL (Fig. 2A-C) was accompanied by a
174 ~30% reduction in the level of rapidly relaxing NPQ (qE) compared to *stn7* (Fig. 2E). The qE
175 in the WT and *psal* started at a level similar to *tap38* when the light intensity is first
176 increased, before gradually transitioning to a level closer to the *stn7* over the course of 10
177 minutes (Fig. 2E). While 1-qL was lower in *tap38* under LL, in HL this mutant showed the
178 highest 1-qL, with WT, *stn7* and *psal* plants all significantly lower, consistent with their
179 higher qE (Fig. 2D and E). Likewise, Φ PSI under HL in *tap38* was significantly lower than
180 *stn7*; with WT and *psal* lying in between (Fig. 2F). Correspondingly in *tap38*, Y(ND) was
181 also significantly lower and Y(NA) higher than in *stn7* after the first 150 seconds of HL (Fig.
182 2G,H). Therefore, *stn7* and *tap38* plants show the opposite behaviour in LL and HL, with
183 LHCII phosphorylation promoting lower Y(NA) in LL and dephosphorylation promoting
184 lower Y(NA) in HL. If a smaller PSI antenna size was beneficial in HL then one would

185 expect *psal* to show a similar Φ PSII compared to *stn7* immediately upon transition from LL
186 to HL. Instead *psal*, like the WT, takes ~8-10 minutes to reach the higher Φ PSII and NPQ
187 and lower 1-qL levels in HL; a timescale consistent with dephosphorylation of LHCII and the
188 transition to larger grana (Fig. 2C-E)³².

189

190 **Influence of grana size and state transitions on ET kinetics**

191 We investigated the difference in Φ PSII between *psal* and *stn7* in LL + FR and reduced
192 efficiency of *tap38* in HL further using dark interval relaxation kinetic (DIRK) analysis of
193 P700, Pc and Fd absorption (Fig. 3)^{42,43}. In these DIRK experiments plants were treated for
194 10 minutes with LL (Fig. 3A), LL + FR (Fig. 3B) or HL (Fig. 3C) to reach the steady state,
195 then illumination was terminated and the ensuing kinetics of Pc and P700 reduction and Fd
196 oxidation were analysed. The LL + FR condition involved 9.5 minutes of LL with the final
197 30 seconds augmented with FR. In LL P700 remained reduced in all plants, while Pc, owing
198 to its lower redox potential, was partially oxidised^{40,44}. In the WT and *tap38* Pc oxidation
199 reached 48% but only 30% in *psal* and *stn7* (Fig. 3A). Lower steady state Pc oxidation in LL
200 is consistent with the lower PSI activity in *psal* and *stn7* as they are locked in State I. In line
201 with the higher Y(NA) in *stn7* and *psal* in LL (Fig. 2H), the steady state Fd reduction level
202 was ~30% compared to ~20% in *tap38* and the WT (Fig. 3A). In LL + FR Pc oxidation level
203 increased to ~60% in WT, *tap38*, *psal* and *stn7* (Fig. 3B). In contrast under LL + FR, P700
204 oxidation was slightly higher at 25% in *stn7* compared to 18-20% in *psal*, WT and *tap38*
205 (Fig. 3B), consistent with the larger Y(ND) observed under these conditions (Fig. 2G). Fd
206 reduction was decreased in LL + FR compared to LL in all plants, although was still higher in
207 *stn7* than in WT and *tap38*, while *psal* was now similar to the latter pair (Fig. 3B). In HL Pc
208 oxidation was ~85% and P700 ~75% in WT, *stn7* and *psal*, however in *tap38* P700 was
209 ~60% oxidised and Pc ~98% oxidised (Fig. 3C). Fd in turn was more reduced in HL in *tap38*

210 (~40%) compared to *stn7*, WT and *psal* (~30%). Therefore, in HL Pc is more oxidised,
211 whereas P700 and Fd are more reduced in *tap38* compared to *stn7*, WT and *psal* (Fig. 2E, G,
212 H and Fig. 3C). This variation in the relationship between the fraction of Pc, P700 and Fd
213 that are oxidised or reduced indicates that the equilibrium constant between these species is
214 altered in *tap38* compared to *stn7*, WT and *psal*. This idea is explored further in Fig. 4 below.

215 The dark relaxation kinetics were next fitted with a single-exponential decay function
216 to obtain the half-time (Extended Data. Fig 4)⁴⁵. In LL + FR the half-time for P700⁺
217 reduction (P700⁺_{red} t_{1/2}) was ~20% shorter for *tap38*, WT and *psal* compared to *stn7* (Fig.
218 3D). In HL P700⁺_{red} t_{1/2} increased by ~20% in the WT and *psal* relative to LL + FR, whereas
219 *stn7* and *tap38* did not show a significant change (Fig. 3D). Thus, P700⁺_{red} t_{1/2} remained
220 significantly shorter in *tap38* in HL compared to *stn7*, WT and *psal* plants (Fig. 3D). A
221 similar picture emerged from analysis of the Pc⁺ half-time (Pc⁺_{red} t_{1/2}) with lower values for
222 the WT, *psal* and *tap38* than *stn7* in LL and LL + FR (Fig. 3E). Under HL, the Pc⁺_{red} t_{1/2}
223 increased to a similar level in the WT and *psal* as in *stn7*, while in *tap38* it remained
224 significantly shorter (Fig. 3E). Under LL, Fd⁻ oxidation (Fd⁻_{ox} t_{1/2}) half-time was shorter in the
225 WT and *tap38* compared to *stn7* and *psal*, whereas in LL +FR *psal* was similar to WT and
226 *tap38*, while *stn7* still lagged behind (Fig. 3F). Under HL, the Fd⁻_{ox} t_{1/2} decreased compared to
227 LL and LL + FR in all plants, although the decrease was significantly smaller in *tap38* (Fig.
228 3F). Increased Y(NA) in *tap38* under HL and *stn7* and *psal* under LL (Fig. 2H) is therefore
229 accompanied by a longer Fd⁻_{ox} t_{1/2} (Fig. 3F).

230 We calculated the initial rate of P700⁺ and Pc⁺ reduction and Fd⁻ oxidation by fitting
231 the first 3-8 ms seconds of the DIRK with a linear function (Extended Data Fig. 4)⁴³. In HL
232 the rate of P700⁺ and Pc⁺ reduction was higher in *tap38* than WT, *stn7* and *psal* (Fig. 3C, E
233 and H). In contrast, under LL+FR Pc⁺ and P700⁺ reduction rates were slower than in HL and
234 now WT, *psal* and *tap38* were similar and faster than *stn7* (Fig. 3G, H). Under LL, Pc⁺

235 reduction rates were fastest in WT and *tap38*, followed by *psal* and then slowest was *stn7*
236 (Fig. 3H). Faster Pc^+ and P700^+ reduction in *tap38* under HL could be explained by the
237 diminished photosynthetic control (Fig. 2G). However, smaller grana in *tap38*, *psal* and WT
238 also increased the rate of reduction of Pc^+ relative to *stn7* under LL conditions, where
239 photosynthetic control is absent (Fig. 3H). Under LL the initial rate of Fd^- oxidation was
240 faster in *tap38* and WT compared to *psal* and *stn7*; *psal* was rescued by FR augmentation,
241 whereas in *stn7* it remained slower (Fig. 3I). Under HL *tap38* showed slower Fd^- oxidation
242 rate despite the higher steady state reduction owing to the longer $\text{Fd}^-_{\text{ox}} t_{1/2}$ (Fig. 3C, F and I).
243 Increased $Y(\text{NA})$ in *stn7* under LL and *tap38* under HL is therefore accompanied by a
244 decrease in Fd^- oxidation rate, which may reflect a lower activity of either or both CET and
245 the CBB.

246

247 **Distinguishing the contributions of ΔpH and grana size**

248 The increase in $\text{P700}^+_{\text{red}}$ and $\text{Pc}^+_{\text{red}} t_{1/2}$ seen in the WT in HL (Fig. 3D and E) is consistent
249 with photosynthetic control of the *cytb₆f* complex by ΔpH in HL^{10,46,47}. The negligible
250 increase in these parameters in HL for *tap38* may therefore indicate a reduced ΔpH in this
251 mutant, which would be in line with the lower q_E and $Y(\text{ND})$ (Fig. 2E, G). Measurement of
252 the proton motive force (*pmf*) using electrochromic shift (ECS) absorption spectroscopy^{48,49}
253 confirmed that the *pmf* was lower in *tap38* in HL compared to *stn7* and WT (*psal* was not
254 determined) (Fig. 4A). In contrast, under LL the *pmf* was slightly, but not significantly, lower
255 in *stn7* compared to WT and *tap38* (Fig. 4A). The assignment of the relative partitioning of
256 the *pmf* into $\Delta\Psi$ and ΔpH using the ECS method remains controversial⁵⁰. Nevertheless, using
257 this method did not yield any differences in the partitioning of the components between WT,
258 *tap38* and *stn7* in HL that might explain the differences (Extended Data Fig. 5A). Indeed, the
259 only difference observed when this method was applied was a smaller ΔpH and higher $\Delta\Psi$ in

260 WT under LL compared to *tap38* and *stn7*. Thus, the increased $Pc^{+}_{red} t^{1/2}$ observed in *stn7*
261 under LL cannot be ascribed to either a higher proportion of ΔpH or total *pmf*. Using a single-
262 turnover flash over a FR background to pre-oxidise PSI, we measured $P700^{+}_{red} t^{1/2}$ in a range
263 of grana size mutants (Fig. 4B). The values for the grana size in each mutant are calculated
264 from previously reported SIM data³². We found a linear positive correlation (slope = 5.197,
265 $r^2 = 0.9$) between grana size and $P700^{+}_{red} t^{1/2}$, with the highest values seen for the *curt1abcd*
266 mutant that has $\sim 1.35 \mu m$ diameter grana and the lowest for the CURT1A overexpressor
267 ($\sim 0.3 \mu m$) (Fig. 4B)^{32,51}. These data indicate that $P700^{+}_{red} t^{1/2}$ may be affected by grana
268 diameter as well as ΔpH . If Pc diffusion is affected by grana diameter then one would expect
269 an effect on the redox equilibration between Pc and $P700$. The equilibrium constant (K_{eq}) for
270 the forward reaction between the $P700/P700^{+}$ and Pc/Pc^{+} redox couples is ~ 81 ⁵⁵. Compared
271 to K_{eq} , an apparent equilibrium constant (K_{app}) of 13.1 was found for the WT under LL + FR
272 conditions (Extended Data Fig. 5B) and just 4.4 under HL conditions (Fig. 4C). This value is
273 much lower than K_{eq} , but in line with previous studies which show there is substantial
274 disequilibrium between Pc and $P700$ *in vivo* and that K_{app} declines with increasing electron
275 flux^{44,52-55}. There was no significant difference in K_{app} values between the mutants in LL +
276 FR conditions (Extended Data Fig. 5B). In contrast in HL, the K_{app} values were significantly
277 different, with *tap38* giving the highest K_{app} and *stn7* the lowest, while WT and *psal* lay in
278 between (Fig 4C). Therefore differences in $Pc/P700$ equilibration between *tap38* and *psal*,
279 WT and *stn7* can explain some of the difference observed in $P700^{+} t^{1/2}$ under HL, but not
280 under LL. Previously the Pc - $P700$ K_{app} was changed upon dark to light transition and
281 attributed to an alteration in lumen thickness⁵³. Using thin-section electron microscopy on LL
282 and HL adapted leaves we examined lumenal sizes under HL and LL, but no significant
283 difference was observed in the WT (Extended Data Fig. 6). Moreover, there was no
284 significant difference between the mutants and WT in HL (Extended Data Fig. 6). These

285 results suggest that differences in K_{app} in HL between WT and the mutants are not due to
286 altered lumen thickness. No differences were found in *cytb₆f* content between the mutants
287 (Extended Data Fig. 7) that might explain the differences either. Another possibility is that
288 the distribution of *cytb₆f* between the grana and stromal lamellae is affected by the LL and
289 HL treatment, but no significant differences were observed between the mutants (Extended
290 Data Fig. 7). The Pc:PSI ratio was lower in *stn7* and *psal* than WT and *tap38* (Extended Data
291 Fig. 3), although since K_{app} was similar in WT and *psal* it suggests that grana size is the
292 dominant factor. Another possibility is that grana size affects PQ/PQH₂ diffusion in the
293 densely crowded thylakoid, which are ~70-80% protein by composition^{56,57}. To investigate
294 this further we subjected LL-adapted WT, *tap38* and *stn7* leaves to a 200 ms saturating flash
295 and followed the subsequent re-oxidation of Q_A⁻ in the dark (Fig. 4D). For Q_A⁻ to be re-
296 oxidised, PQ must bind to the Q_B-site of PSII. After the flash, PQ is regenerated by oxidation
297 of PQH₂ at the oxidising site of *cytb₆f*. In *stn7* the half-time of Q_A⁻ re-oxidation (Q_A⁻_{ox} t_{1/2}) is
298 significantly increased compared to *psal*, *tap38* and WT in LL-adapted leaves, consistent
299 with a retarded diffusion of PQH₂ between PSII and *cytb₆f* in this mutant (Fig. 4D). However,
300 HL treatment increased Q_A⁻_{ox} t_{1/2} of the *psal*, WT to a similar level as *stn7*, although *tap38*
301 was still faster (Fig. 4D). Therefore, the differences in PQ/PQH₂ diffusion can explain the
302 variation in the P700⁺_{red} t_{1/2} LL+FR and part of that in HL, while differences in Pc diffusion/
303 equilibration also contribute to the differences in HL.

304

305 **Influence of grana size and state transitions on CET**

306 Since the Y(NA) phenotype of *stn7* under LL and *tap38* under HL were similar, we probed
307 this parameter in more detail across a range of light intensities and found a cross-over at ~800
308 μmol photons m⁻² s⁻¹ (Fig. 5A). At light intensities below this value *tap38* shows lower
309 Y(NA) than *stn7*, while above this intensity the opposite is true. In contrast the WT Y(NA)

310 remains comparatively low under all conditions (Fig. 5A)^{40,58,59}. We investigated whether
311 HL treatment resulted in detectable damage to PSI by assessing the ECS a-phase amplitude in
312 leaves infiltrated with DCMU. Compared to dark-adapted leaves HL treated leaves showed
313 no-significant reduction in functional PSI for *stn7* and WT, however *tap38* showed a
314 significant reduction of ~10-15%, confirming PSI suffers light induced damage in this mutant
315 (Extended Data Fig. 8A).

316 We next compared the difference in estimated PSI and PSII electron transfer rates
317 inferred by chlorophyll fluorescence and P700 absorption spectroscopy respectively against
318 light intensity ($\Delta ETR(I) = ETR(I) - ETR(II)$), with excess PSI turnover reflecting the
319 contribution of CET and/or PSI charge recombination (Fig. 5B)⁶⁰⁻⁶². The estimated ETR(I)
320 and ETR(II) values were corrected for each mutant based on the partitioning of light between
321 the photosystems determined by their relative antenna sizes (Extended Data Figure 1) and the
322 absorptivity of each leaf measured using an integrating sphere. In the WT $\Delta ETR(I)$ increases
323 from 0 to ~600 $\mu\text{mol photons m}^{-2} \text{ s}^{-1}$ before declining slightly between 600 and 1500 μmol
324 $\text{photons m}^{-2} \text{ s}^{-1}$ (Fig. 5B). Infiltration of the WT with 1 mM methyl viologen, a PSI electron
325 acceptor that abolishes CET, suppressed $\Delta ETR(I)$ at all but the lowest light intensities (Fig.
326 5B). In comparison to *stn7*, the $\Delta ETR(I)$ for *tap38* was significantly higher at light intensities
327 below 250 $\mu\text{mol photons m}^{-2} \text{ s}^{-1}$, although markedly lower at light intensities above ~600
328 $\mu\text{mol photons m}^{-2} \text{ s}^{-1}$ (Fig 5B). The data suggest that *stn7* and WT plants have increased
329 CET capacity in HL relative to *tap38*, and that *tap38* has a higher capacity under LL (Fig.
330 5B). We tested this idea further by infiltrating leaves with the CBB cycle inhibitor
331 iodoacetamide (IA), which irreversibly modifies sulfhydryl groups inactivating the CBB
332 cycle enzymes⁶³. It has been shown previously that IA insulates the CET system against
333 electron loss, allowing the activity of the cyclic system to be measured with FR
334 illumination⁶³. We found no difference in gH^+ between the mutants that might suggest a

335 differential sensitivity to IA (Extended Data Fig. 8B). Leaves of WT and *stn7* plants
336 infiltrated with 4 mM IA and illuminated with FR showed higher levels of *pmf* than *tap38*,
337 consistent with the higher capacity for CET (Fig. 5C), under conditions where the electron
338 transfer chain is largely reduced⁶³. Finally, we tested the idea that higher Y(NA) in LL in *stn7*
339 and in HL in *tap38* is due to a smaller electron sink capacity by comparing leaves infiltrated
340 with either 20 mM Hepes pH 7.5, 150 mM sorbitol, 50 mM NaCl (buffer) or buffer with
341 NaCl replaced by 50 mM NaNO₂. The NO₂⁻ ion is reduced in the chloroplast stroma into
342 NH₄⁺, thus consuming electrons and potentially boosting the electron sink capacity. NaNO₂
343 caused a marked reduction in Y(NA) in *stn7* under LL and in *tap38* under HL relative to the
344 buffer control lowering this parameter to WT levels in each case (Fig. 5D). We tested
345 whether NO₂⁻ reduction in the chloroplast led to uncoupling through accumulation of NH₄⁺ in
346 the chloroplast by comparing the levels of rapidly-reversible ΔpH dependent NPQ (qE) in
347 NaNO₂ versus buffer infiltrated leaves (Extended Data Fig. 8C). In fact, the results showed
348 that NO₂⁻ slightly enhanced qE, probably due to higher LET, suggesting accumulation of
349 NH₄⁺ is insufficient to cause significant uncoupling.

350

351 **Discussion**

352 Dynamic thylakoid stacking adjusts membrane architecture to changes in light intensity and
353 spectral quality, yet its exact function has remained unclear³⁰⁻³⁴. We previously observed that
354 changing grana diameter affected P700⁺_{red} t_{1/2} in flash absorption spectroscopy experiments³³.
355 Here we observed the same in the steady state using DIRK; P700 reduction was faster when
356 grana are smaller and slower when grana were larger. Control of P700⁺_{red} t_{1/2} by ΔpH -
357 dependent regulation of the rate of PQH₂ oxidation by *cytb₆f* is well established^{45,46,64}.
358 However, since grana diameter affected P700⁺_{red} t_{1/2} under LL, where ΔpH is small and
359 indistinguishable between *tap38* and *stn7*, as well as in HL, its effect is independent and

360 additive. Changes in the relative levels of *cytb₆f* and its lateral distribution between mutants
361 can be excluded as possible causes since these were not detected. The impact of grana
362 diameter on LET is further corroborated by its positive linear correlation with $P700^{+}_{red} t^{1/2}$ that
363 we observe in the single-turnover flash experiments (Fig. 4B). In principle, faster reduction
364 of $P700^{+}$ may result from faster Pc or PQ/PQH₂ diffusion within the membrane. Under LL,
365 $Q_{A^{-}ox} t^{1/2}$ was significantly shorter in WT, *tap38* and *psal* plants with smaller grana than in
366 *stn7* with larger grana. This finding is consistent with previous reports comparing low light
367 and dark-adapted thylakoids and spinach leaves which showed that PQ/PQH₂ migration
368 within the membrane primarily occurs within nanodomains in the grana and that diffusion
369 between grana and stromal lamellae is much slower^{56,65,66}. We suggest under conditions
370 where the PQ pool is relatively more oxidised, competition between PQ and PQH₂ for
371 binding the oxidising site of *cytb₆f* can limit LET⁶⁷. Shortening the diffusion distance from
372 granal PSII to stromal *cytb₆f* via smaller grana would ameliorate this by effectively increasing
373 the concentration of *cytb₆f* involved in LET. However, we found this beneficial effect of
374 smaller grana under LL is only realised in steady-state measurements when the limitation on
375 P700 oxidation is first removed by state transitions or FR augmentation. Therefore, the
376 advantage of *psal*, which possesses smaller grana in LL but is locked in State I, over *stn7*
377 which possesses large grana and is locked in State I is only seen under FR illumination (Fig.
378 2C). Under HL, in addition to altered PQ/PQH₂ diffusion evidenced by a lower $Q_{A^{-}ox} t^{1/2}$ in
379 *tap38* compared to the WT, *stn7* and *psal* (Fig. 4D), Pc diffusion also appears to play a
380 significant role. A clear difference is seen in Pc-P700 K_{app} between the mutants, with *tap38*
381 showing significantly higher K_{app} compared to *stn7*, WT and *psal* (Fig. 4C). Lower Pc-PSI
382 K_{app} could either reflect altered Pc/PSI ratios or slower diffusion between Pc and PSI due to
383 increased distance between granal *cytb₆f* and stromal PSI^{33,55} or a narrower lumen⁵³. A
384 decreased Pc/PSI ratio is observed in *stn7* and *psal*, however since the latter behaves like WT

385 in both LL and HL this change appears to have little effect. The relative insensitivity of K_{app}
386 to Pc/PSI ratio is consistent with the higher accumulation of Pc in *Arabidopsis* compared
387 to other species where Pc levels correlate well with LET capacity⁶⁸. Indeed, a 80-90%
388 decrease in Pc levels due to PETE2 knock-out in *Arabidopsis* had little effect on LET⁶⁹.
389 Since lumen width was not significantly different between the mutants, alterations in grana
390 diameter are implicated in variations in K_{app} , consistent with recent results on the *curt1abcd*
391 mutant⁵⁵. Interestingly, little change in K_{app} is observed between the mutants under LL
392 conditions. Therefore, the effect of increased grana diameter on Pc diffusion and Pc-P700
393 equilibration may only be felt under HL conditions when the high-potential chain is oxidised.
394 The benefit of larger grana to steady state LET rate can be clearly seen by comparison of *psal*
395 and *stn7*, in the former the transition to higher Φ_{PSII} is gradual (Fig. 2C) despite this mutant
396 already being in State I. Therefore a smaller PSI antenna size in HL does not appear to
397 provide a benefit to LET efficiency, a finding compatible with the fact that P700 is a strong
398 excitation quencher irrespective of its redox state and is thus unlikely to be damaged by over-
399 excitation⁷⁰.

400 Remarkably, the symptoms of lower $^{14}CO_2$ and Φ_{PSII} in *stn7* under LL and *tap38*
401 under HL were similar, both showing an over-reduction of the PSI acceptor side (Fig. 5A). In
402 the case of *tap38* this translated into damage to PSI upon prolonged 2 hour HL treatment
403 (Extended Data Fig. 8A). In the steady state, Y(NA) is maintained in the WT at a low level
404 (< 0.2) and the Fd pool redox state shows a consistent reduction of ~25-30% under both LL
405 and HL conditions (Fig. 3A-C), in line with recent reports^{40,71}. Clearly the Fd redox state is
406 quite tightly controlled within narrow limits in the steady state (Fig. 3F). An increase in
407 Y(NA) i.e. the accumulation of electrons on the acceptor side of PSI reflects a mismatch
408 between the rate of Fd oxidation (Fig. 3I) and the rate of its reduction by PSI. Consistent with
409 this Y(NA) could be lowered in *stn7* under LL and *tap38* under HL by infiltration of leaves

410 with nitrite, which acts as an electron acceptor in the chloroplast stroma (Fig. 5D). The
411 balance between Fd oxidation and reduction is regulated at the PSI acceptor-side by the
412 activity of downstream electron sinks such as the CBB cycle and CET, and at the PSI donor-
413 side by photosynthetic control⁷². This normal pattern of PSI acceptor-side regulation is
414 disrupted when state transitions in LL and/ or transition to increased grana size in HL are lost.
415 How much of these mutant phenotypes can be explained by mis-regulation of LET alone or
416 by CET (with subsequent effects on LET) deserves consideration. On one hand in *tap38*
417 under HL, the higher Y(NA) could be explained by a partial loss of photosynthetic control
418 due to lower ΔpH (Fig. 4A), faster PQH₂ diffusion and a higher Pc-PSI K_{app} (Fig. 4C).
419 Similarly, in *stn7* under LL the higher Y(NA) could reflect an increased rate of LET that is
420 mismatched with the capacity of the CBB cycle to consume electrons. However, in our view
421 this ‘LET only’ explanation is inconsistent with several elements of our data: i) in *stn7* under
422 LL both ΦPSII and $^A\text{CO}_2$ are lower confirming that LET is inhibited rather than enhanced; ii)
423 the ability of FR light to decrease Y(NA) and increase LET under LL, iii) in *tap38* under HL
424 and in *stn7* under LL we observe a decrease in $\Delta\text{ETR(I)}$, indicating lower CET capacity, in
425 each case (Fig. 5B).

426 An alternative more consistent with the data is therefore a combined ‘LET *and* CET’
427 explanation i.e. we suggest that both photosynthetic control *and* acceptor-side regulation
428 through CET both play a role in the observed Y(NA) phenotype. This idea is further
429 corroborated by the recent work of Shikanai and co-workers who found the higher Y(NA)
430 observed in the *pgr5* mutant involved mis-regulation of both donor- and acceptor-side
431 regulation⁵⁸. The ability of CET to limit Y(NA) is based on its ability to augment ΔpH
432 production by LET. The ‘extra’ ΔpH can be utilised by the ATP synthase to increase ATP
433 concentration in the stroma. The CBB requires 1.5 ATP/ NADPH, which given the 4.67
434 H⁺/ATP ratio inferred by the structure of the chloroplast ATP synthase indicates a ATP

435 shortfall of ~ 0.32 ATP/ NADPH from LET alone⁷³. The situation is complicated by the
436 multitude of other metabolic process in the stroma consuming ATP and NADPH in different
437 ratios⁷², however the flexibility in the provision of ATP relative to NADPH provided by CET
438 appears to be crucial to plant fitness⁷⁴. Thus, the high Y(NA) phenotype of *stn7* under LL and
439 *tap38* under HL could be explained by a shortfall in ATP due to lower CET that in turn leads
440 to a reduced CBB activity. The resulting slower regeneration of NADP⁺ would of course also
441 lead to decreased Φ PSII, as is observed. A requirement for CET generated Δ pH to augment
442 ATP levels for maximising CBB cycle activity seems more likely in LL where *pmf* is non-
443 saturated (Fig. 4A). However, under HL there is evidence that substantial disequilibrium
444 exists between *pmf* and the phosphorylation potential^{75,76}, thus here CET may serve a purely
445 regulatory role both removing electrons from the PSI acceptor-side and downregulating the
446 donor-side through Δ pH production. This would be consistent with the higher *pmf* in *stn7*
447 compared to *tap38* under HL, but no reciprocal effect in LL (since additional *pmf* in *tap38* is
448 consumed through ATP production) (Fig. 4A).

449 What is the cause of lower CET in *stn7* under LL and *tap38* under HL? Saliiently, we
450 observed that under LL conditions Y(NA) and Fd reduction level can be lowered and Φ PSII
451 increased by augmentation of PSI excitation with FR light in *psal* and *stn7* (Fig. 2C, H and
452 Fig. 3B). This effect was largely missing in *tap38* and WT plants, which adopt State II in LL
453 conditions (constitutively in the case of *tap38*). Increasing PSI excitation will increase the
454 ratio of PSI to PSII turnover, and thus CET relative to LET. Thus in LL, under-excitation of
455 PSI would appear to be the primary cause of lower CET, consistent with previous data in
456 plants and *Chlamydomonas* linking transition to State II with increased CET capacity²⁴⁻²⁷.
457 Alternatively, to lower CET in LL, the smaller restorative effect of FR light on Φ PSII in *stn7*
458 compared to *psal* (Fig. 2C), may be explained by the slower PQ/PQH₂ diffusion in the former
459 due to its larger grana size (Fig. 4D). Indeed, this effect would likely mitigate the stimulatory

460 effect of FR by slowing both LET and CET, thus lowering the amount of extra ATP synthesis
461 it provokes. Under HL, CET no longer appears to be limited by PSI excitation since $\Delta\text{ETR(I)}$
462 it smaller in *tap38* despite the fact it possesses the largest PSI antenna (Fig. 5B, Extended
463 Data Fig. 1). Instead, we observed that in all plants the $\Delta\text{ETR(I)}$ is increasingly suppressed as
464 light intensity increases, although the extent of suppression is greatest in *tap38* (Fig 5B). This
465 suppression is consistent with the experimentally demonstrated requirement of CET for redox
466 poise^{52,63,77}. Previously, we obtained evidence that the larger grana observed in HL can assist
467 CET by slowing the reduction of the stromal PQ pool by PSII thus maintaining proper redox
468 posing of the CET pathway³³. A similar effect of PQ compartmentalisation between grana
469 and stromal lamellae was previously observed by Joliot et al⁶⁵. Thus, under HL CET is likely
470 limited by availability of oxidised PQ in the stroma. Here we provide further evidence for
471 this view showing that under HL $\Delta\text{ETR(I)}$ is higher in both *stn7* and WT, where grana are
472 larger relative to *tap38*. It is striking that the symptoms of *tap38* in HL are a milder version of
473 those reported for *pgr5* mutant, which is compromised in the major CET pathway⁷⁴. Similar
474 to *tap38*, *pgr5* shows lower LET and lower $\Delta\text{ETR(I)}$ in HL, together with reduced ΔpH ,
475 lower Y(ND), increased Y(NA) and PSI photoinhibition^{22,58}. There is evidence that PGR5
476 might either act directly as part of a Fd-PQ reductase with PGRL1⁸ or alternatively as a
477 regulatory element within a FNR-Fd-cyt b_6/f complex^{10,78}. Thus, Fd reduction of PQ in HL
478 would be the limiting step in both *pgr5* and *tap38* mutants. Indeed, since the *pgr5* mutant also
479 fails to dephosphorylate LHCII in HL⁷⁹, and thus likely retains small grana in HL, it may be
480 crippled in two separate aspects of CET regulation.

481 The results in this study provide a basis for finally reconciling the role of LHCII
482 phosphorylation with regulation of CET. When the CBB cycle is limited by ATP in LL, the
483 resultant accumulation of NADPH and reduced Fd will increase Y(NA) and thus cause
484 reduction of the electron transfer chain upstream of PSI, including the PQ pool. STN7 is

485 activated by reduction of the PQ pool and LHCII phosphorylation triggers a transition to
486 smaller grana and State II. Increased PSI excitation relative to PSII increases the rate of CET
487 relative to LET and this provides extra ΔpH to increase ATP synthesis. In contrast in HL,
488 when the CBB cycle is limited primarily by CO₂ availability, NADPH, reduced Fd *and* ATP
489 accumulate. The latter factor is crucial since high ATP levels cause ΔpH to increase
490 inhibiting STN7¹⁸, despite the presence of a reduced PQ pool. The ensuing TAP38-
491 dependent dephosphorylation LHCII triggers a transition to larger grana and State I, which
492 facilitates increased CET by isolating the stromal PQ pool from PSII, poising it for CET. This
493 synergy in the action of LHCII phosphorylation in LL and dephosphorylation in HL in
494 promoting CET may be missing in green algae such as *Chlamydomonas*. To date dynamic
495 thylakoid stacking changes have not yet been observed in *Chlamydomonas* and indeed the
496 strict stacking of the membranes observed in higher plants is missing⁸⁰. Another point of
497 difference is that in *Chlamydomonas*, a supercomplex containing PSI, LHCII, *cytb₆f*, PGRL1,
498 Fd and FNR is observed under conditions that promote CET^{28,81}. It is possible that this CET
499 supercomplex serves the same role as larger grana in higher plants, i.e. compartmentalising
500 PQ for the CET pathway⁸¹.

501 In conclusion, we have established that dynamic thylakoid stacking regulates
502 photosynthetic electron transfer independent of state transitions, demonstrating they have a
503 synergistic function in plants in regulating the PSI acceptor-side. Given the importance of
504 STN7 to plant fitness¹⁹⁻²² and since *tap38* plants were previously shown to grow faster than
505 WT under controlled LL conditions¹⁴, engineering crop plants to have constitutively high
506 LHCII phosphorylation was considered a possible route to higher yield. However, our results
507 show that dephosphorylation of LHCII serves a crucial photoprotective function in HL.
508 Therefore, such a strategy is unlikely to yield success and a more nuanced approach is
509 required.

510

511 **Materials & Methods**

512 **Plant Material**

513 *Arabidopsis* plants were grown for 5 weeks in a Conviron plant growth room with an 8-hour
514 photoperiod at a light intensity of 200 $\mu\text{mol photons m}^{-2} \text{s}^{-1}$ and day/night temperatures of
515 22/18 °C, respectively.

516

517

518 **Structured illumination microscopy (SIM)**

519 *Arabidopsis* was imaged on a DeltaVision OMX V4 microscope (GE Healthcare) equipped
520 with the Blaze-3D SIM module and 60x 1.42 NA oil planapochromat lens. Chlorophyll
521 fluorescence was excited with a 642 nm laser and the emission was collected through a
522 683/40 nm bandpass filter. The structured illumination pattern was projected onto the sample
523 in a series of five phases for each of three angles leading to a total of 15 images per axial
524 slice. The 3D image was acquired via sectioning with a 2D slice separation of 125 nm. The
525 final super-resolution image was reconstructed with SoftWoRx OMX v6.0 software (GE
526 Healthcare). Grana diameter was measured as the full-width half-maximum of a line profile
527 across the granal-midpoint in images that had been thresholded and 16-bit converted with the
528 SIMcheck plugin for ImageJ (v153).

529

530 **Low-temperature fluorescence spectroscopy.**

531 Thylakoid membranes were prepared according to Järvi *et al.*, 2011, from *Arabidopsis* leaves
532 either adapted to LL (125 $\mu\text{mol photons m}^{-2} \text{s}^{-1}$) or HL (1150 $\mu\text{mol photons m}^{-2} \text{s}^{-1}$). 1 μM of
533 chlorophyll from thylakoids was suspended in the fluorescence buffer (60% glycerol, 300 mM
534 sucrose, 5 mM MgCl_2 , 20 mM HEPES pH 7.8) and measured in 1 cm polymethyl methacrylate

535 cuvettes in a Opistat liquid nitrogen cooled bath cryostat (Oxford Instruments). Fluorescence
536 emission measurements were performed as previously described using a FluoroLog FL3-22
537 spectrofluorimeter (Jobin Yvon)³².

538

539 **Spectroscopic determination of chlorophylls and cytochromes.**

540 Spectroscopic assay of P700⁸³ and *cytb₆*⁸⁴ content was performed on isolated thylakoids.

541 Grana and stromal lamellae were prepared as described previously⁸⁵.

542

543 **Gas exchange**

544 A LICOR-6800 portable photosynthesis system was used to carry out infrared gas analysis
545 (IRGA) on a fully expanded leaf while still attached to the plant. Relative humidity inside
546 the IRGA chamber was kept at 60% to 65% using self-indicating desiccant, the flow rate was
547 set at 150 $\mu\text{mol s}^{-1}$, and leaf temperature at 20°C. Reference [CO₂] was maintained at 400
548 ppm. After being matched, plants were allowed to equilibrate for 40 to 45 min inside
549 the IRGA chamber. Once readings were stable, measurements were taken every 30 s for 10
550 min. Stomatal counts were performed as described⁸⁶.

551

552 **Chlorophyll fluorescence and *in situ* P700, Pc and Fd absorption spectroscopy.**

553 Pulse-amplitude modulated chlorophyll fluorescence and P700, Pc and Fd absorption
554 spectroscopy were measured using a Dual-KLAS-NIR photosynthesis analyser (Walz)⁴² or
555 Imaging-PAM and associated software (v2.072). Maximum levels of Fd, Pc and P700
556 absorption were determined on leaves via induction of full oxidation (Pc, P700) or full
557 reduction (Fd) and deconvolution by model spectra in NIR region^{40,42,52}. For DIRK
558 experiments the traces were normalised such that the maximally oxidised/reduced state
559 (100%) was set using the maximum absorption obtainable using the method of Klughammer
560 and Schreiber, 2016. Pc/P700 and Fd/P700 ratios (Extended Data Fig. 3) are represented as a
561 relative values using the same procedure⁴². Chlorophyll fluorescence parameters and relative
562 Pc, P700 and Fd redox state were determined at each light intensity using a 6 $\mu\text{mol photons}$
563 $\text{s}^{-1} \text{m}^{-2}$ modulated measuring light (540 nm) in combination with a saturating pulse of 18000
564 $\mu\text{mol photons m}^{-2} \text{s}^{-1}$. Actinic light was provided in the ratio of 10% 460 nm, 90% 635 nm.
565 Far-red light (740nm), was provided at an intensity of 255 $\mu\text{mol photons m}^{-2} \text{s}^{-1}$. Chlorophyll
566 fluorescence and P700 parameters were calculated as previously described^{41,87}. The

567 estimated electron transport rate through PSI and PSII (ETR(I) and ETR (II)) was calculated
568 using the formulae: $ETR(I) = \Phi_{PSI} \times I$ (light intensity) $\times PFDa$ (absorbed light) $\times PR$
569 (fraction light partitioned PSI), $ETR(II) = \Phi_{PSII} \times I$ (light intensity) $\times PFDa \times PR$ (fraction
570 light partitioned PSII). $PFDa$ was calculated using an integrating sphere and PR from the data
571 in Extended Data Fig. 1, applying the LL partition values to light intensities below 600 μmol
572 photons $\text{m}^{-2} \text{s}^{-1}$ and HL values to those above. The half-time for Pc, P700 and Fd redox
573 changes was calculated by fitting a single exponential function to the DIRK (Fig. 3A-C) or
574 flash data (Fig 4B, D)⁴⁵. The initial slope (Fig. 3G, H, I) of DIRK was determined using a
575 linear fit applied between 3 ms and 8 ms into the dark interval as this was determined to be a
576 short enough window to give a reliable estimate (i.e. the slope was linear during this period
577 (see Extended Data Fig. 4). The equilibrium constant (K_{eq}) for the forward reaction between
578 the P700/P700⁺ and Pc/Pc⁺ redox couples is ~81 as calculated from their respective midpoint
579 potentials (P700/P700⁺ $E'_m = 475$ mV, Pc/Pc⁺ $E'_m = 362$ mV)⁵⁵. Compared to K_{eq} the
580 apparent equilibrium constant (K_{app}) may be derived from the slope of the equilibrium plots
581 derived from the DIRK data (Fig. 4C and Extended Data Fig. 5B)^{40,42,52}. Single-turnover
582 measurements (Fig. 4B, Extended Data Fig. 8A) were performed using a 50 μs flash (18000
583 μmol photons $\text{m}^{-2} \text{s}^{-1}$, 635 nm light), for Fig 4A a far-red background light (255 μmol photons
584 $\text{m}^{-2} \text{s}^{-1}$, 740 nm) was also applied, 10 flashes per sample were averaged. Data analysed with
585 Graphpad Prism v9.

586

587 **ECS absorption spectroscopy.**

588 The ECS signal was measured on leaves using a Walz Dual-PAM fitted with a P515/535
589 emitter module⁴⁸. The proton conductance gH^+ (Extended Data Figs. 5C, 8B) and *pmf* (Fig.
590 4A, 5C) parameters were determined as previously described⁸⁸.

591

592 **Infiltration**

593 Leaves vacuum infiltrated with either 1mM methyl viologen (Fig 5B), 4 mM Iodoacetamide
594 (IA) (Fig 5C and Extended Data Fig 6B), 30 μM 3-(3,4-dichlorophenyl)-1,1-dimethylurea
595 (DCMU) (Extended Data Fig. 1 and Extended Data Fig. 8A) or 50 mM NaNO_2 (Fig. 5D and
596 Extended Data Fig. 8C), buffered in 20 mM Hepes pH 7.5, 150 mM sorbitol, 50 mM NaCl
597 (NaCl excluded for NaNO_2 infiltration).

598

599 **Electron Microscopy**

600 Thin-section EM was performed on leaves as previously described ³³

601

602 **Data availability**

603 The datasets analysed during the current study are available from the corresponding author on

604 reasonable request. The sequence data from this article can be found in The Arabidopsis

605 Information Resource or GenBank/EMBL database under the following accession numbers:

606 STN7 (At1g68830), TAP38/PPH1 (At4t27800), CURT1A (At4g01150), CURT1B

607 (At2g46820), CURT1C (At1g52220), CURT1D (At4g38100), PSAL (At4g12800).

608

609 **Acknowledgments**

610 We wish to thank Professor Dario Leister (LMU Munich) and Dr Mathias Pribil

611 (Copenhagen Plant Science Center) for providing seeds of the *psal*, *curt1abcd*, *oeCURT1A*

612 and *tap38* lines and Professor Lutz Eichacker (University of Stavenger) for providing seeds

613 of *stn7*. Chris Hill (University of Sheffield) is acknowledged for assistance with the EM.

614 M.P.J. acknowledges funding from the Leverhulme Trust grants RPG-2016-161 and RPG-

615 2019-045 and the BBSRC White Rose DTP for a studentship to TEM (BB/M011151/1). The

616 SIM imaging was performed at the University of Sheffield Wolfson Light Microscopy

617 Facility and was partly funded by MRC Grant MR/K015753/1.

618 **Author Contributions**

619 M.P.J. and S.C. designed the study; C.H., W.H.J.W., T.Z.EM and M.S.P performed the

620 research; C.H., W.H.J.W., T.Z.EM and M.P.J. analysed the data; M.P.J. C.H., W.H.J.W.,

621 T.Z.EM S.C. and M.S.P wrote the paper.

622 **Ethics Declaration**

623 Competing Interests

624 The authors declare no competing interests

625

626 **References**

- 627 1. Ruban, A. V. Evolution under the sun: Optimizing light harvesting in photosynthesis. *J.*
628 *Exp. Bot.* (2015) doi:10.1093/jxb/eru400.
- 629 2. Miyake, C. Molecular mechanism of oxidation of p700 and suppression of ROS
630 production in photosystem I in response to electron-sink limitations in C3 plants.
631 *Antioxidants* **9**, 230 (2020).
- 632 3. Li, Z., Wakao, S., Fischer, B. B. & Niyogi, K. K. Sensing and Responding to Excess Light.
633 *Annu. Rev. Plant Biol.* (2009) doi:10.1146/annurev.arplant.58.032806.103844.
- 634 4. Ruban, A. V., Johnson, M. P. & Duffy, C. D. P. The photoprotective molecular switch in
635 the photosystem II antenna. *Biochim. Biophys. Acta - Bioenerg.* **1817**, 167–181 (2012).
- 636 5. Suorsa, M. *et al.* PGR5 ensures photosynthetic control to safeguard photosystem I
637 under fluctuating light conditions. *Plant Signal. Behav.* e22741 (2013)
638 doi:10.4161/psb.22741.
- 639 6. Johnson, G. N. Physiology of PSI cyclic electron transport in higher plants. *Biochim.*
640 *Biophys. Acta - Bioenerg.* **1807**, 384–389 (2011).
- 641 7. Yamori, W. & Shikanai, T. Physiological Functions of Cyclic Electron Transport Around
642 Photosystem I in Sustaining Photosynthesis and Plant Growth. *Annu. Rev. Plant Biol.*
643 **67**, 81–106 (2016).
- 644 8. Hertle, A. P. *et al.* PGRL1 Is the Elusive Ferredoxin-Plastoquinone Reductase in
645 Photosynthetic Cyclic Electron Flow. *Mol. Cell* (2013)
646 doi:10.1016/j.molcel.2012.11.030.
- 647 9. Nandha, B., Finazzi, G., Joliot, P., Hald, S. & Johnson, G. N. The role of PGR5 in the
648 redox poisoning of photosynthetic electron transport. *Biochim. Biophys. Acta - Bioenerg.*
649 **1767**, 1252–1259 (2007).
- 650 10. Joliot, P. & Johnson, G. N. Regulation of cyclic and linear electron flow in higher
651 Plants. *Proc. Natl. Acad. Sci. U. S. A.* **108**, 13317–13322 (2011).
- 652 11. Allen, J. F. State transitions - A question of balance. *Science* (2003)

- 653 doi:10.1126/science.1082833.
- 654 12. Ruban, A. V. & Johnson, M. P. Dynamics of higher plant photosystem cross-section
655 associated with state transitions. *Photosynth. Res.* **99**, 173–183 (2009).
- 656 13. Bellaflore, S., Barneche, F., Peltler, G. & Rochaix, J. D. State transitions and light
657 adaptation require chloroplast thylakoid protein kinase STN7. *Nature* **433**, 892–895
658 (2005).
- 659 14. Shapiguzov, A. *et al.* The PPH1 phosphatase is specifically involved in LHCII
660 dephosphorylation and state transitions in Arabidopsis. *Proc. Natl. Acad. Sci. U. S. A.*
661 (2010) doi:10.1073/pnas.0913810107.
- 662 15. Pribil, M., Pesaresi, P., Hertle, A., Barbato, R. & Leister, D. Role of plastid protein
663 phosphatase TAP38 in LHCII dephosphorylation and thylakoid electron flow. *PLoS*
664 *Biol.* (2010) doi:10.1371/journal.pbio.1000288.
- 665 16. Vener, A. V., Van Kan, P. J. M., Rich, P. R., Ohad, I. & Andersson, B. Plastoquinol at the
666 quinol oxidation site of reduced cytochrome *b_f* mediates signal transduction between
667 light and protein phosphorylation: Thylakoid protein kinase deactivation by a single-
668 turnover flash. *Proc. Natl. Acad. Sci. U. S. A.* **94**, 1585–1590 (1997).
- 669 17. Rintamäki, E., Martinsuo, P., Pursiheimo, S. & Aro, E. M. Cooperative regulation of
670 light-harvesting complex II phosphorylation via the plastoquinol and ferredoxin-
671 thioredoxin system in chloroplasts. *Proc. Natl. Acad. Sci. U. S. A.* **97**, 11644–11649
672 (2000).
- 673 18. Fernyhough, P., Foyer, C. H. & Horton, P. Increase in the level of thylakoid protein
674 phosphorylation in maize mesophyll chloroplasts by decrease in the transthylakoid
675 pH gradient. *FEBS Lett.* **176**, 133–138 (1984).
- 676 19. Taylor, C. R., Van Ieperen, W. & Harbinson, J. Demonstration of a relationship
677 between state transitions and photosynthetic efficiency in a higher plant. *Biochem. J.*
678 (2019) doi:10.1042/BCJ20190576.
- 679 20. Frenkel, M. *et al.* Improper excess light energy dissipation in Arabidopsis results in a
680 metabolic reprogramming. *BMC Plant Biol.* (2009) doi:10.1186/1471-2229-9-12.
- 681 21. Külheim, C., Ågren, J. & Jansson, S. Rapid regulation of light harvesting and plant
682 fitness in the field. *Science (80-.)*. **297**, 91–93 (2002).
- 683 22. Suorsa, M. *et al.* PROTON GRADIENT REGULATION5 is essential for proper acclimation
684 of Arabidopsis photosystem I to naturally and artificially fluctuating light conditions.

- 685 *Plant Cell* **24**, 2934–2948 (2012).
- 686 23. Lunde, C., Jensen, P. E., Haldrup, A., Knoetzel, J. & Scheller, H. V. The PSI-H subunit of
687 photosystem I is essential for state transitions in plant photosynthesis. *Nature* (2000)
688 doi:10.1038/35046121.
- 689 24. Fernyhough, P., Foyer, C. & Horton, P. The influence of metabolic state on the level of
690 phosphorylation of the light-harvesting chlorophyll-protein complex in chloroplasts
691 isolated from maize mesophyll. *BBA - Bioenerg.* (1983) doi:10.1016/0005-
692 2728(83)90235-9.
- 693 25. Allen, J. F. Protein phosphorylation - Carburettor of photosynthesis? *Trends Biochem.*
694 *Sci.* **8**, 369–373 (1983).
- 695 26. Cardol, P. *et al.* Impaired respiration discloses the physiological significance of state
696 transitions in *Chlamydomonas*. *Proc. Natl. Acad. Sci. U. S. A.* **15**, 15979–15984 (2009).
- 697 27. Bulté, L., Gans, P., Rebéillé, F. & Wollman, F. A. ATP control on state transitions in vivo
698 in *Chlamydomonas reinhardtii*. *BBA - Bioenerg.* (1990) doi:10.1016/0005-
699 2728(90)90095-L.
- 700 28. Takahashi, H., Clowez, S., Wollman, F. A., Vallon, O. & Rappaport, F. Cyclic electron
701 flow is redox-controlled but independent of state transition. *Nat. Commun.* **4**, 1954
702 (2013).
- 703 29. Pesaresi, P. *et al.* Arabidopsis STN7 kinase provides a link between short- and long-
704 term photosynthetic acclimation. *Plant Cell* **21**, 2402–2423 (2009).
- 705 30. Kyle, D. J., Staehelin, L. A. & Arntzen, C. J. Lateral mobility of the light-harvesting
706 complex in chloroplast membranes controls excitation energy distribution in higher
707 plants. *Arch. Biochem. Biophys.* **222**, 527–541 (1983).
- 708 31. Rozak, P. R., Seiser, R. M., Wacholtz, W. F. & Wise, R. R. Rapid, reversible alterations
709 in spinach thylakoid appression upon changes in light intensity. *Plant Cell Environ.*
710 (2002).
- 711 32. Wood, W. H. J., Barnett, S. F. H., Flannery, S., Hunter, C. N. & Johnson, M. P. Dynamic
712 thylakoid stacking is regulated by LHCII phosphorylation but not its interaction with
713 PSI. *Plant Physiol.* **180**, 2152–2166 (2019).
- 714 33. Wood, W. H. J. *et al.* Dynamic thylakoid stacking regulates the balance between linear
715 and cyclic photosynthetic electron transfer. *Nat. Plants* **4**, 116–127 (2018).
- 716 34. Anderson, J. M., Horton, P., Kim, E. H. & Chow, W. S. Towards elucidation of dynamic

- 717 structural changes of plant thylakoid architecture. *Philosophical Transactions of the*
718 *Royal Society B: Biological Sciences* (2012) doi:10.1098/rstb.2012.0373.
- 719 35. Capretti, A. *et al.* Nanophotonics of higher-plant photosynthetic membranes. *Light*
720 *Sci. Appl.* (2019) doi:10.1038/s41377-018-0116-8.
- 721 36. Grieco, M., Tikkanen, M., Paakkanen, V., Kangasjärvi, S. & Aro, E. M. Steady-state
722 phosphorylation of light-harvesting complex II proteins preserves photosystem I
723 under fluctuating white light. *Plant Physiol.* **160**, 1896–1910 (2012).
- 724 37. Tikkanen, M., Grieco, M., Kangasjärvi, S. & Aro, E. M. Thylakoid protein
725 phosphorylation in higher plant chloroplasts optimizes electron transfer under
726 fluctuating light. *Plant Physiol.* (2010) doi:10.1104/pp.109.150250.
- 727 38. Tikkanen, M. *et al.* State transitions revisited—a buffering system for dynamic low
728 light acclimation of *Arabidopsis*. *Plant Mol. Biol.* (2006) doi:10.1007/s11103-006-
729 9088-9.
- 730 39. Pribil, M., Labs, M. & Leister, D. Structure and dynamics of thylakoids in land plants.
731 *Journal of Experimental Botany* (2014) doi:10.1093/jxb/eru090.
- 732 40. Schreiber, U. & Klughammer, C. Analysis of photosystem I donor and acceptor sides
733 with a new type of online-deconvoluting kinetic LED-array spectrophotometer. *Plant*
734 *Cell Physiol.* (2016) doi:10.1093/pcp/pcw044.
- 735 41. Klughammer, C. & Schreiber, U. An improved method, using saturating light pulses,
736 for the determination of photosystem I quantum yield via P700⁺-absorbance changes
737 at 830 nm. *Planta* (1994) doi:10.1007/BF00194461.
- 738 42. Klughammer, C. & Schreiber, U. Deconvolution of ferredoxin, plastocyanin, and P700
739 transmittance changes in intact leaves with a new type of kinetic LED array
740 spectrophotometer. *Photosynth. Res.* (2016) doi:10.1007/s11120-016-0219-0.
- 741 43. Sacksteder, C. A. & Kramer, D. M. Dark-interval relaxation kinetics (DIRK) of
742 absorbance changes as a quantitative probe of steady-state electron transfer.
743 *Photosynth. Res.* (2000) doi:10.1023/A:1010785912271.
- 744 44. Kirchhoff, H., Schöttler, M. A., Maurer, J. & Weis, E. Plastocyanin redox kinetics in
745 spinach chloroplasts: Evidence for disequilibrium in the high potential chain. *Biochim.*
746 *Biophys. Acta - Bioenerg.* **1659**, 63–72 (2004).
- 747 45. Ott, T., Clarke, J., Birks, K. & Johnson, G. Regulation of the photosynthetic electron
748 transport chain. *Planta* (1999) doi:10.1007/s004250050629.

- 749 46. Jahns, P., Graf, M., Munekage, Y. & Shikanai, T. Single point mutation in the Rieske
750 iron-sulfur subunit of cytochrome b6/f leads to an altered pH dependence of
751 plastoquinol oxidation in Arabidopsis. *FEBS Lett.* **519**, 99–102 (2002).
- 752 47. Correa Galvis, V. *et al.* H⁺ Transport by K⁺ EXCHANGE ANTIporter3 Promotes
753 Photosynthesis and Growth in Chloroplast ATP Synthase Mutants. *Plant Physiol.*
754 (2020) doi:10.1104/pp.19.01561.
- 755 48. Klughammer, C., Siebke, K. & Schreiber, U. Continuous ECS-indicated recording of the
756 proton-motive charge flux in leaves. *Photosynth. Res.* (2013) doi:10.1007/s11120-
757 013-9884-4.
- 758 49. Sacksteder, C. A., Kanazawa, A., Jacoby, M. E. & Kramer, D. M. The proton to electron
759 stoichiometry of steady-state photosynthesis in living plants: A proton-pumping Q
760 cycle is continuously engaged. *Proc. Natl. Acad. Sci. U. S. A.* **97**, 14283–14288 (2000).
- 761 50. Johnson, M. P. & Ruban, A. V. Rethinking the existence of a steady-state $\Delta\psi$
762 component of the proton motive force across plant thylakoid membranes.
763 *Photosynth. Res.* (2014) doi:10.1007/s11120-013-9817-2.
- 764 51. Armbruster, U. *et al.* Arabidopsis CURVATURE THYLAKOID1 proteins modify thylakoid
765 architecture by inducing membrane curvature. *Plant Cell* (2013)
766 doi:10.1105/tpc.113.113118.
- 767 52. Schreiber, U. Redox changes of ferredoxin, P700, and plastocyanin measured
768 simultaneously in intact leaves. *Photosynth. Res.* (2017) doi:10.1007/s11120-017-
769 0394-7.
- 770 53. Kirchhoff, H. *et al.* Dynamic control of protein diffusion within the granal thylakoid
771 lumen. *Proc. Natl. Acad. Sci. U. S. A.* (2011) doi:10.1073/pnas.1104141109.
- 772 54. Joliot, P. & Joliot, A. Electron transfer between the two photosystems. II. Equilibrium
773 constants. *BBA - Bioenerg.* (1984) doi:10.1016/0005-2728(84)90016-1.
- 774 55. Höhner, R. *et al.* Plastocyanin is the long-range electron carrier between photosystem
775 II and photosystem I in plants. *Proc. Natl. Acad. Sci. U. S. A.* (2020)
776 doi:10.1073/pnas.2005832117.
- 777 56. Kirchhoff, H., Horstmann, S. & Weis, E. Control of the photosynthetic electron
778 transport by PQ diffusion microdomains in thylakoids of higher plants. *Biochim.*
779 *Biophys. Acta - Bioenerg.* **1459**, 148–168 (2000).
- 780 57. Kirchhoff, H., Mukherjee, U. & Galla, H. J. Molecular architecture of the thylakoid

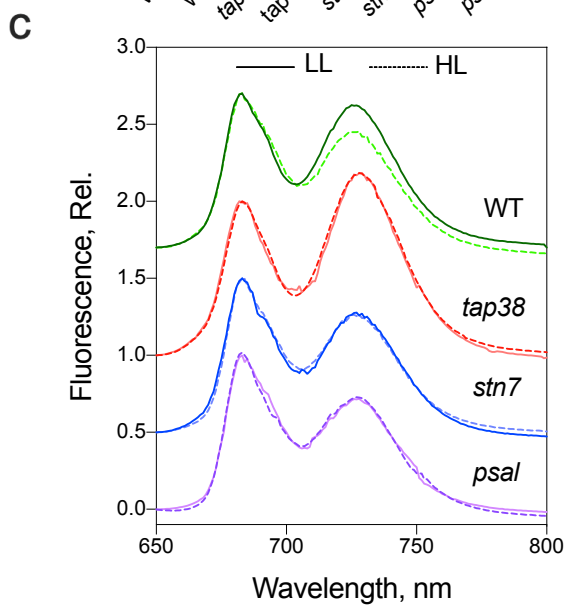
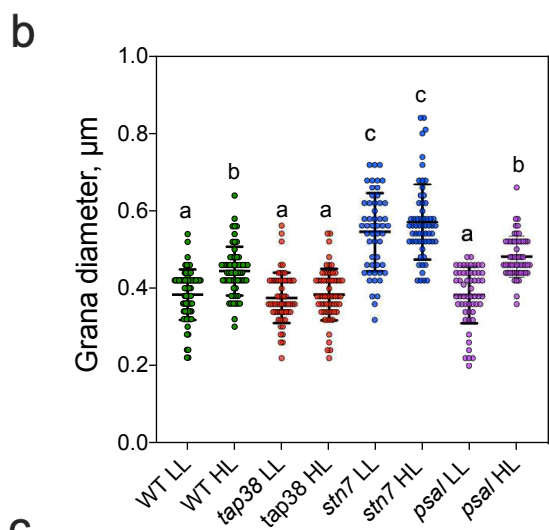
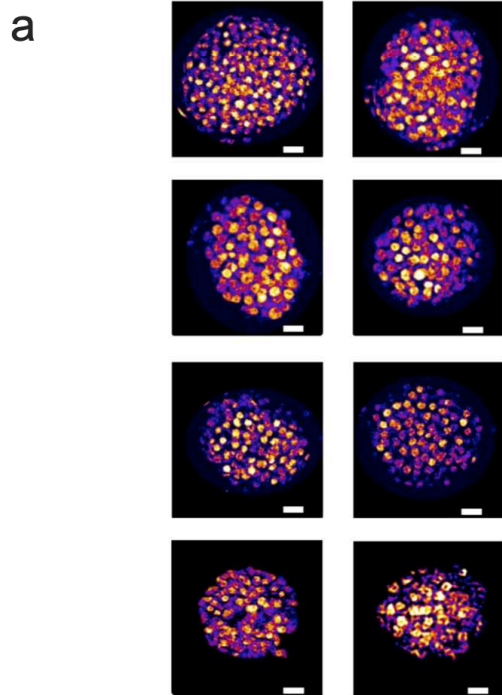
- 781 membrane: Lipid diffusion space for plastoquinone. *Biochemistry* (2002)
782 doi:10.1021/bi011650y.
- 783 58. Yamamoto, H. & Shikanai, T. PGR5-dependent cyclic electron flow protects
784 photosystem I under fluctuating light at donor and acceptor sides. *Plant Physiol.* **179**,
785 588–600 (2019).
- 786 59. Barbato, R. *et al.* Higher order photoprotection mutants reveal the importance of
787 Δ pH-dependent photosynthesis-control in preventing light induced damage to both
788 photosystem II and photosystem I. *Sci. Rep.* **10**, 1 (2020).
- 789 60. Kou, J., Takahashi, S., Fan, D. Y., Badger, M. R. & Chow, W. S. Partially dissecting the
790 steady-state electron fluxes in photosystem I in wild-type and pgr5 and ndh mutants
791 of arabidopsis. *Front. Plant Sci.* (2015) doi:10.3389/fpls.2015.00758.
- 792 61. Kadota, K. *et al.* Oxidation of P700 induces alternative electron flow in photosystem I
793 in wheat leaves. *Plants* (2019) doi:10.3390/plants8060152.
- 794 62. Nawrocki, W. J. *et al.* Maximal cyclic electron flow rate is independent of PGRL1 in
795 *Chlamydomonas*. *Biochim. Biophys. Acta - Bioenerg.* **1860**, 425–432 (2019).
- 796 63. Joliot, P. & Alric, J. Inhibition of CO₂ fixation by iodoacetamide stimulates cyclic
797 electron flow and non-photochemical quenching upon far-red illumination.
798 *Photosynth. Res.* (2013) doi:10.1007/s11120-013-9826-1.
- 799 64. Nishio, J. N. & Whitmarsh, J. Dissipation of the proton electrochemical potential in
800 intact chloroplasts. *Plant Physiol.* (1993) doi:10.1104/pp.101.1.89.
- 801 65. Joliot, P., Lavergne, J. & Béal, D. Plastoquinone compartmentation in chloroplasts. I.
802 Evidence for domains with different rates of photo-reduction. *Biochim. Biophys. Acta*
803 *- Bioenerg.* **1101**, 1–12 (1992).
- 804 66. Johnson, M. P., Vasilev, C., Olsen, J. D. & Hunter, C. N. Nanodomains of cytochrome
805 b6f and photosystem II complexes in spinach grana thylakoid membranes. *Plant Cell*
806 **26**, 3051–3061 (2014).
- 807 67. Tikhonov, A. N. The cytochrome b6f complex at the crossroad of photosynthetic
808 electron transport pathways. *Plant Physiol. Biochem.* **81**, 163–183 (2014).
- 809 68. Schöttler, M. A. & Tóth, S. Z. Photosynthetic complex stoichiometry dynamics in
810 higher plants: environmental acclimation and photosynthetic flux control. *Front. Plant*
811 *Sci.* **5**, 188 (2014).
- 812 69. Pesaresi, P. *et al.* Mutants, overexpressors, and interactors of arabidopsis

- 813 plastocyanin isoforms: Revised roles of plastocyanin in photosynthetic electron flow
814 and thylakoid redox state. *Mol. Plant* (2009) doi:10.1093/mp/ssn041.
- 815 70. Tiwari, A. *et al.* Photodamage of iron-sulphur clusters in photosystem i induces non-
816 photochemical energy dissipation. *Nat. Plants* (2016) doi:10.1038/NPLANTS.2016.35.
- 817 71. Takagi, D. & Miyake, C. PROTON GRADIENT REGULATION 5 supports linear electron
818 flow to oxidize photosystem I. *Physiol. Plant.* (2018) doi:10.1111/ppl.12723.
- 819 72. Foyer, C. H., Neukermans, J., Queval, G., Noctor, G. & Harbinson, J. Photosynthetic
820 control of electron transport and the regulation of gene expression. *J. Exp. Bot.* **63**,
821 1637–1661 (2012).
- 822 73. Kramer, D. M. & Evans, J. R. The Importance of Energy Balance in Improving
823 Photosynthetic Productivity. *Plant Physiol.* **155**, 70–78 (2011).
- 824 74. Munekage, Y. *et al.* Cyclic electron flow around photosystem I is essential for
825 photosynthesis. *Nature* **429**, 579–582 (2004).
- 826 75. Giersch, C. *et al.* Energy charge, phosphorylation potential and proton motive force in
827 chloroplasts. *BBA - Bioenerg.* (1980) doi:10.1016/0005-2728(80)90146-2.
- 828 76. Backhausen, J. E., Kitzmann, C., Horton, P. & Scheibe, R. Electron acceptors in isolated
829 intact spinach chloroplasts act hierarchically to prevent over-reduction and
830 competition for electrons. *Photosynth. Res.* (2000) doi:10.1023/A:1026523809147.
- 831 77. Slovacek, R. E., Mills, J. D. & Hind, G. The function of cyclic electron transport in
832 photosynthesis. *FEBS Lett.* (1978) doi:10.1016/0014-5793(78)80136-7.
- 833 78. Buchert, F., Mosebach, L., Gäbelein, P. & Hippler, M. PGR5 is required for efficient Q
834 cycle in the cytochrome b6f complex during cyclic electron flow. *Biochem. J.* **477**,
835 1631–1650 (2020).
- 836 79. Mekala, N. R., Suorsa, M., Rantala, M., Aro, E. M. & Tikkanen, M. Plants actively avoid
837 state transitions upon changes in light intensity: Role of light-harvesting complex ii
838 protein dephosphorylation in high light. *Plant Physiol.* **168**, 721–734 (2015).
- 839 80. Engel, B. D. *et al.* Native architecture of the chlamydomonas chloroplast revealed by
840 in situ cryo-electron tomography. *Elife* (2015) doi:10.7554/eLife.04889.
- 841 81. Iwai, M. *et al.* Isolation of the elusive supercomplex that drives cyclic electron flow in
842 photosynthesis. *Nature* **464**, 1210–1213 (2010).
- 843 82. Järvi, S., Suorsa, M., Paakkarinen, V. & Aro, E. M. Optimized native gel systems for
844 separation of thylakoid protein complexes: Novel super- and mega-complexes.

- 845 *Biochem. J.* (2011) doi:10.1042/BJ20102155.
- 846 83. Melis, A. Kinetic analysis of P-700 photoconversion: Effect of secondary electron
847 donation and plastocyanin inhibition. *Arch. Biochem. Biophys.* (1982)
848 doi:10.1016/0003-9861(82)90535-5.
- 849 84. Metzger, S. U., Cramer, W. A. & Whitmarsh, J. Critical analysis of the extinction
850 coefficient of chloroplast cytochrome f. *Biochim. Biophys. Acta - Bioenerg.* (1997)
851 doi:10.1016/S0005-2728(96)00164-8.
- 852 85. Fristedt, R. *et al.* Phosphorylation of photosystem II controls functional macroscopic
853 folding of photosynthetic membranes in *Arabidopsis*. *Plant Cell* (2009)
854 doi:10.1105/tpc.109.069435.
- 855 86. Hepworth, C., Doheny-Adams, T., Hunt, L., Cameron, D. D. & Gray, J. E. Manipulating
856 stomatal density enhances drought tolerance without deleterious effect on nutrient
857 uptake. *New Phytol.* (2015) doi:10.1111/nph.13598.
- 858 87. Maxwell, K. & Johnson, G. N. Chlorophyll fluorescence - A practical guide. *Journal of*
859 *Experimental Botany* (2000) doi:10.1093/jxb/51.345.659.
- 860 88. Huang, W., Suorsa, M. & Zhang, S. B. In vivo regulation of thylakoid proton motive
861 force in immature leaves. *Photosynth. Res.* (2018) doi:10.1007/s11120-018-0565-1.
- 862 89. Malkin, S., Armond, P. A., Mooney, H. A. & Fork, D. C. Photosystem II Photosynthetic
863 Unit Sizes from Fluorescence Induction in Leaves. *Plant Physiol.* (1981)
864 doi:10.1104/pp.67.3.570.

865

866 **Figure legends**



868

869 **Figure 1 | Changes in thylakoid grana diameter and excitation energy distribution**

870 **between photosystems in LL and HL. a**, Representative SIM images of *Arabidopsis* WT,

871 *stn7*, *tap38*, and *psal* mutants induced by 1 h of low light (LL, 125 $\mu\text{mol photons m}^{-2} \text{s}^{-1}$) or

872 high light (HL, 1150 $\mu\text{mol photons m}^{-2} \text{s}^{-1}$), Scale bars 1 μm . Two independent sets of

873 images were obtained with similar results. **b**, Mean grana diameter (FWHM of fluorescence

874 signal) in each sample \pm SD (n (number of grana analysed) = 66, 62, 54, 60, 60, 60, 55, 56 in

875 order of presentation from left to right); the letters a, b and c represent significant differences

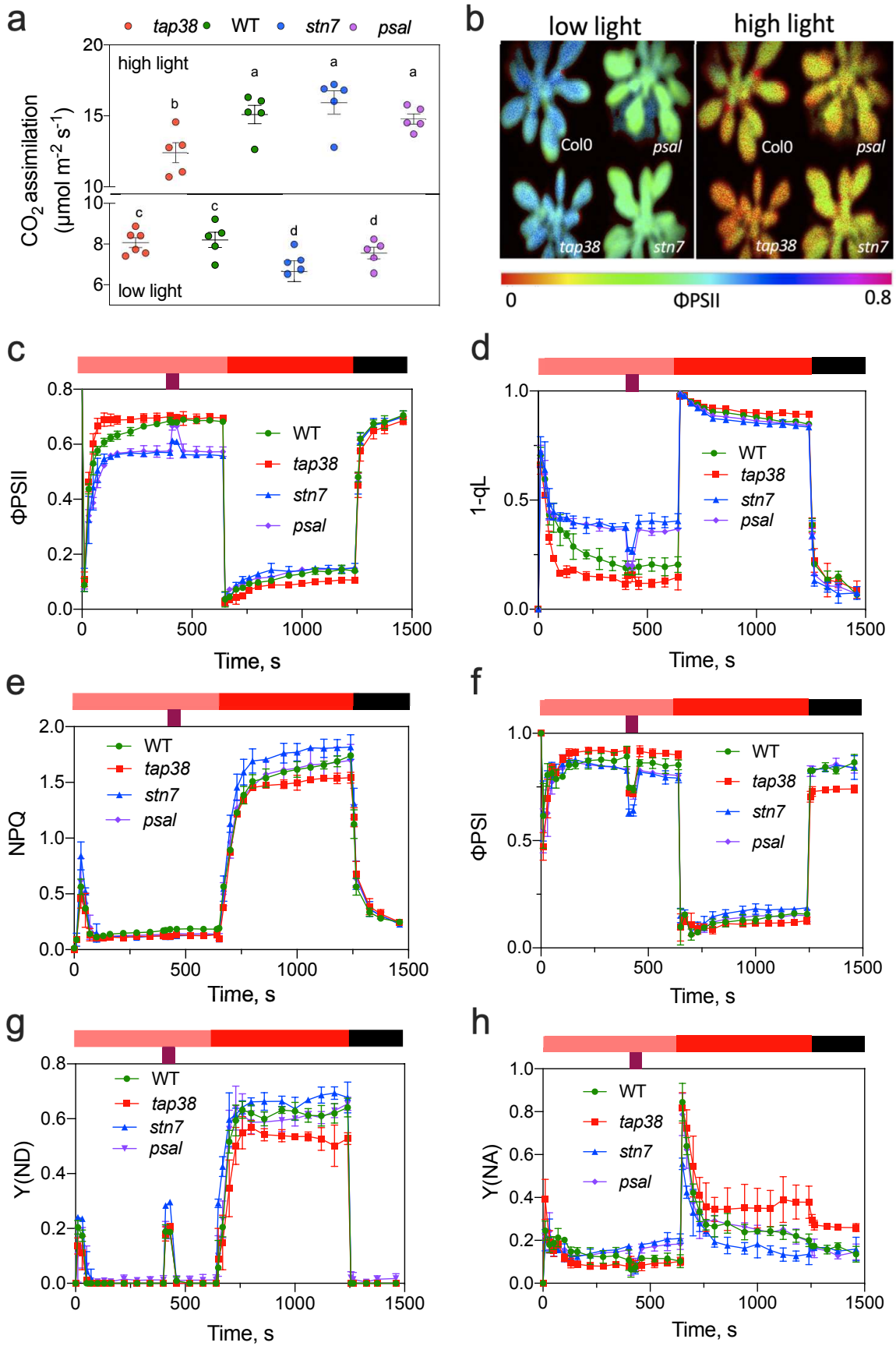
876 calculated using one-way analysis of variance (ANOVA) with Tukey's multiple comparisons

877 test, a-b $P=0.0001$, a-c $P<0.0001$, b-c $P<0.0001$. **c**, Stacked 77 K fluorescence emission

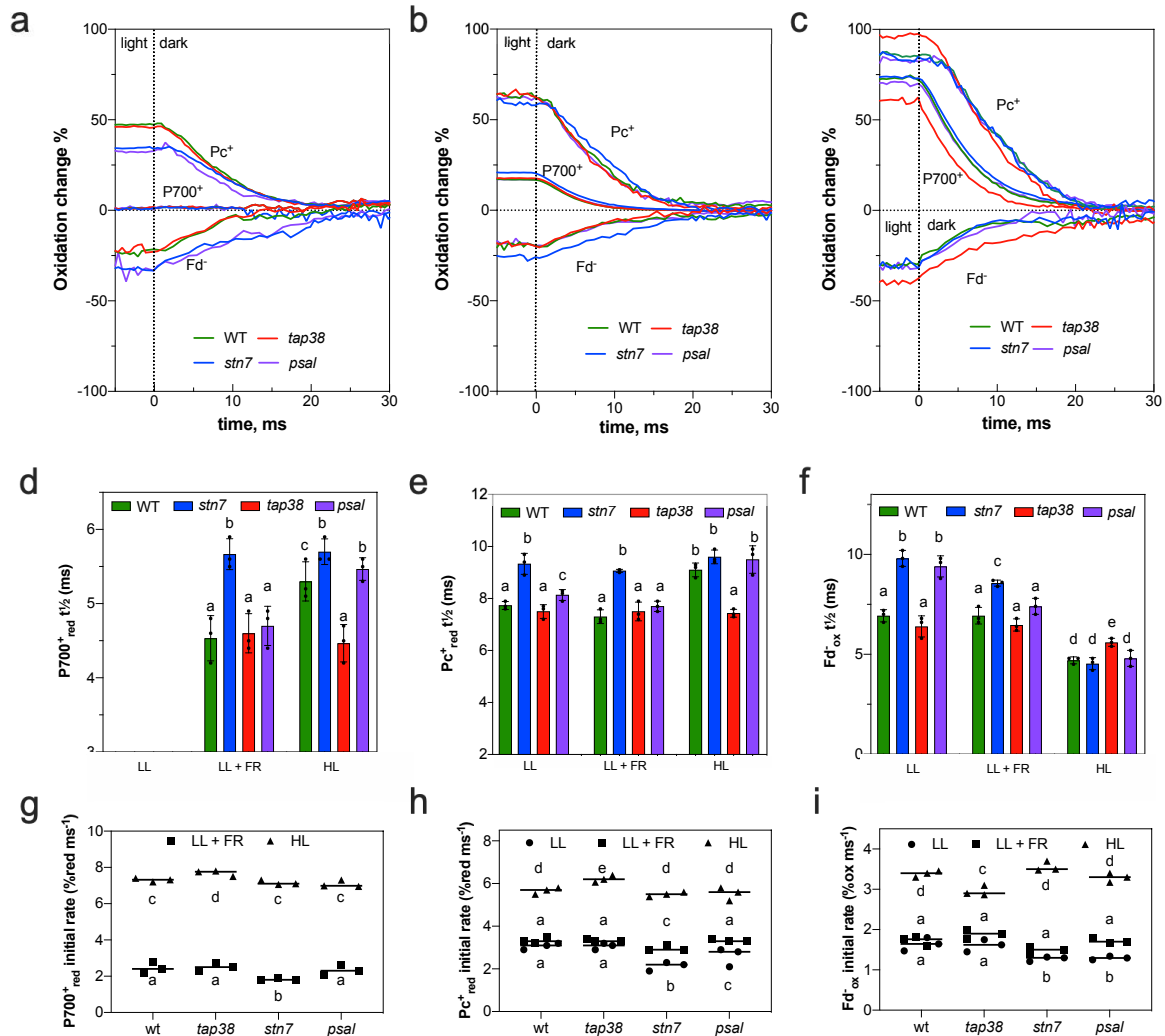
878 spectra (435 nm excitation) of thylakoids prepared from each sample following 1 h of LL

879 (solid lines) or HL (dashed lines) treatment. Pairs of spectra (LL, HL) were normalised to 685

880 nm.



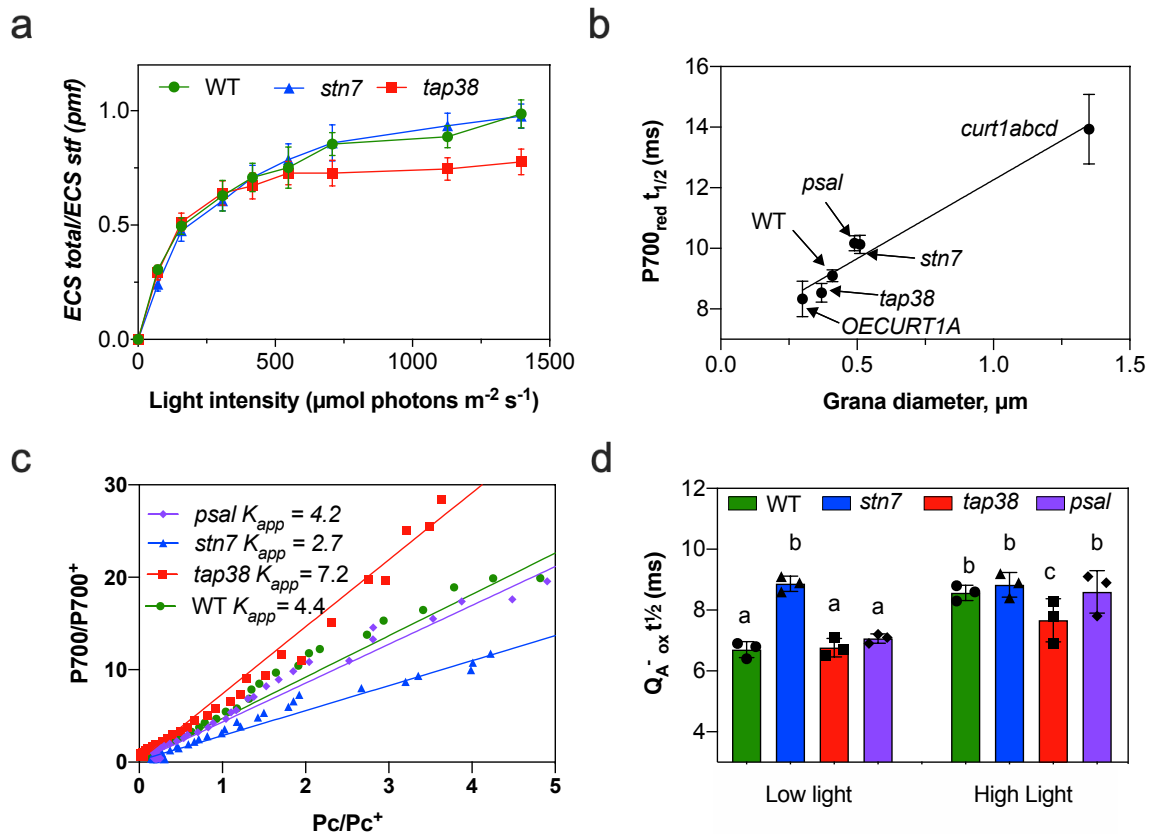
882 **Figure 2 | Photosynthetic properties of WT, *tap38*, *stn7* and *psal* *Arabidopsis* plants**
883 **determined by infra-red gas exchange, chlorophyll fluorescence and P700 absorption**
884 **spectroscopy. a**, CO₂ assimilation (^ACO₂) measured on each sample following 1 hour of low
885 light (LL, 125 μmol photons m⁻² s⁻¹) or high light (HL, 1150 μmol photons m⁻² s⁻¹)
886 illumination. The letters a, b, c and d represent significant differences calculated using one-
887 way analysis of variance (ANOVA) with Tukey's multiple comparisons test, a-b P= 0.0009,
888 a-c P=<0.0001, a-d P=<0.0001, b-c P=<0.0001, b-d P=<0.0001, c-d P=0.0009. **b**,
889 Representative chlorophyll fluorescence images showing PSII quantum yield (ΦPSII) under
890 LL and HL in each sample. **c**, Kinetics of ΦPSII under 10 minutes LL (pale red bar)
891 including 30 s augmentation with far-red light (740 nm, 255 μmol photons m⁻² s⁻¹, burgundy
892 bar) and 10 minutes HL (bright red bar), followed by 4 minutes dark recovery in each sample
893 (black bar). **d**, 1-qL (PSII acceptor side limitation), **e**, Non-photochemical quenching (NPQ),
894 **f**, Quantum yield of PSI (ΦPSI), **g**, PSI donor-side limitation (Y(ND)), **h**, PSI acceptor-side
895 limitation (Y(NA)). n (separate plants analysed) = 5-6 for each sample; mean ± SD is shown
896 for each timepoint.



897

898 **Figure 3 | Dark interval relaxation kinetic analysis of the reduction PSI (P700⁺), P_c⁺ and**
 899 **oxidation of F_d⁻.** **a**, DIRK analysis in leaves from each sample exposed to 10 minutes low
 900 light (LL, 125 μmol photons m⁻² s⁻¹). **b**, DIRK analysis in leaves from each sample exposed
 901 to 10 minutes LL augmented for the final 30 seconds prior to dark interval with far-red light
 902 (740 nm, 255 μmol photons m⁻² s⁻¹). **c**, DIRK analysis in leaves from each sample exposed to
 903 10 minutes high light (HL, 1150 μmol photons m⁻² s⁻¹). **d**, P700⁺ reduction half-time
 904 calculated from single exponential fit of kinetics in a-c. The letters a-c represent significant
 905 differences calculated using one-way analysis of variance (ANOVA) with Tukey's multiple
 906 comparisons test, a-b P=<0.0001, a-c P=<0.0001, b-c P=0.0358. **e**, P_c⁺ reduction half-time
 907 calculated from single exponential fit of kinetics in a-c. The letters a-c represent significant

908 differences calculated using one-way analysis of variance (ANOVA) with Tukey's multiple
909 comparisons test, a-b $P < 0.0001$, a-c $P = 0.0106$, b-c $P < 0.0001$. **f**, Fd^+ oxidation half-time
910 calculated from single exponential fit of kinetics in a-c. The letters a-e represent significant
911 differences calculated using one-way analysis of variance (ANOVA) with Tukey's multiple
912 comparisons test, a-b $P < 0.0001$, a-c $P = 0.0001$, a-d $P < 0.0001$, a-e $P < 0.0001$, b-c $P = 0.046$,
913 b-d $P < 0.0001$, b-e $P < 0.0001$, c-d $P < 0.0001$, c-e $P < 0.0001$, d-e $P = 0.024$. **g**, Initial rate
914 of P700^+ reduction calculated from linear fit of kinetics in the 3-8 ms window in a-c. The
915 letters a-d represent significant differences calculated using one-way analysis of variance
916 (ANOVA) with Tukey's multiple comparisons test, a-b $P = 0.0001$, a-c $P < 0.0001$, b-c
917 $P < 0.0001$, b-d $P < 0.0001$, c-d $P = 0.008$. **h**, Initial rate of Pc^+ reduction calculated from
918 linear fit of kinetics in the 3-8 ms window in a-c. The letters a-d represent significant
919 differences calculated using one-way analysis of variance (ANOVA) with Tukey's multiple
920 comparisons test, a-b $P = 0.0001$, a-c $P = 0.033$, a-d $P < 0.0001$, a-e $P < 0.0001$, b-c $P = 0.027$, b-
921 d $P < 0.0001$, b-e $P < 0.0001$, c-d $P < 0.0001$, c-e $P < 0.0001$, d-e $P = 0.016$. **i**, Initial rate of
922 Fd^+ oxidation calculated from linear fit of kinetics in the 3-8 ms window in a-c. The letters a-
923 d represent significant differences calculated using one-way analysis of variance (ANOVA)
924 with Tukey's multiple comparisons test, a-b $P = 0.038$, a-c $P < 0.0001$, a-d $P < 0.0001$, b-c
925 $P < 0.0001$, b-d $P < 0.0001$, c-d $P = 0.0001$. n (separate plants analysed) = 3 for each sample
926 in Fig 3; mean \pm SD is shown.



927

928 **Figure 4 | Investigating possible causes of defective electron transfer regulation in *stn7***

929 **and *tap38*.** **a**, Light-intensity dependence of total proton motive force (ECS total). The ECS

930 total levels were standardised against the 515-nm absorbance change induced by a single

931 turnover flash (ECS stf). **b**, Relationship between P700⁺ reduction half-time following a

932 single-turnover flash (50 μs, 635 nm) applied on a far-red light background (740 nm, 255

933 μmol photons m⁻² s⁻¹). **c**, Equilibrium plot of P700/P700⁺ versus Pc/Pc⁺ from dark interval

934 relaxation kinetics after high light treatment shown in Fig 3C. Apparent equilibrium constants

935 (K_{app}) were calculated from a linear fit of the slope, R values for the linear fits were WT =

936 0.968, *stn7* = 0.982, *tap38* = 0.973 and *psal* 0.974 . **d**, Q_A⁻ oxidation half-time derived from

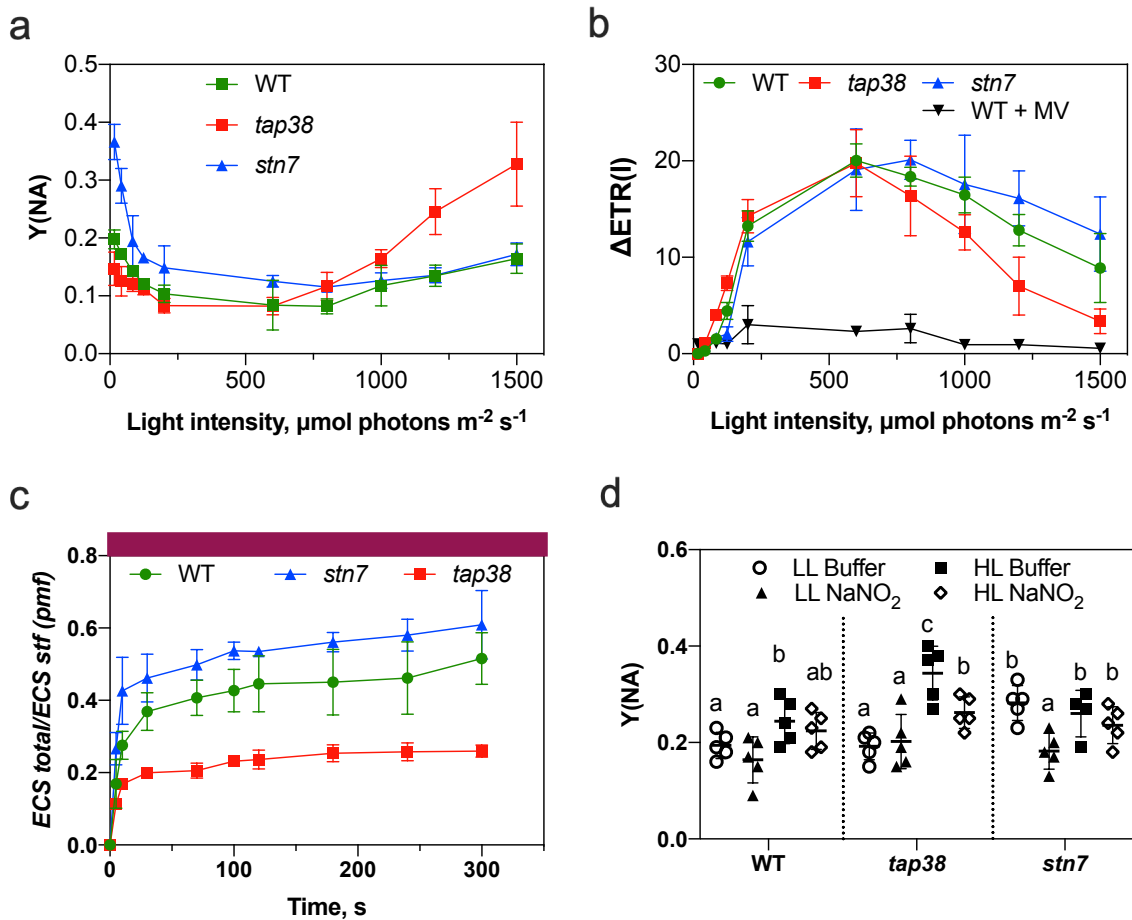
937 decay of PSII chlorophyll fluorescence signal following a 200 ms saturating pulse applied to

938 leaves treated for 1 hour with low light (125 μmol photons m⁻² s⁻¹) or high light (1150 μmol

939 photons m⁻² s⁻¹). The letters a-d represent significant differences calculated using one-way

940 analysis of variance (ANOVA) with Tukey's multiple comparisons test, a-b P=<0.0001, a-c

941 $P < 0.0001$, b-c $P = 0.012$. n (separate plants analysed) = 3 for each sample in Fig 4; mean \pm
 942 SD is shown.



943

944 **Figure 5 | Comparison of PSI acceptor side limitation and cyclic electron transfer. a,**

945 Light-intensity dependence of PSI acceptor side limitation (Y(NA)). n (separate plants

946 analysed) = 3 for each sample; mean \pm SD is shown for each point. **b,** Light-intensity

947 dependence of the difference in estimated electron transfer rate between PSI and PSII

948 ($\Delta\text{ETR(I)} = \text{ETR(I)} - \text{ETR(II)}$). n (separate plants analysed) = 5-6 for each sample; mean \pm SD

949 is shown for each point. **c,** Kinetics of proton motive force formation (ECS total) induced by

950 5 minutes illumination with far-red light (740 nm , $255 \mu\text{mol photons m}^{-2} \text{s}^{-1}$, burgundy bar)

951 on leaves infiltrated with 4mM iodoacetamide. n (separate plants analysed) = 3 for each

952 sample; mean \pm SD is shown for each point. The ECS total levels were standardised against

953 the 515-nm absorbance change induced by a single turnover flash (ECS stf). **d,** Y(NA) after

954 10 minutes illumination in low light (LL, $125 \mu\text{mol photons m}^{-2} \text{s}^{-1}$) or high light (HL,
955 $1150 \mu\text{mol photons m}^{-2} \text{s}^{-1}$) in leaves infiltrated with either 20 mM Hepes pH 7.5, 150 mM
956 sorbitol, 50 mM NaCl (buffer) or buffer with NaCl replaced by 50 mM NaNO_2 . n (separate
957 plants analysed) = 5 for each sample; mean \pm SD is shown for each point. The letters a-d
958 represent significant differences calculated using one-way analysis of variance (ANOVA)
959 with Tukey's multiple comparisons test, a-b $P=0.0001$, a-c $P=<0.0001$, b-c $P=<0.0001$.